Chapter 1

Introduction

An exponentially growing demand for materials, advanced in terms of directional-multi-functionality of the physical properties, has been observed in modern days nanoelectronics. Here the term 'directional' specifies the anisotropy of the physical properties within the microstructure, which implies that the single component made of such materials is expected to show various combinations of the physical properties, such as multi-magnetic [1], multiferroic [2], optoelectronic [3], thermoelectric [4], etc., along different crystallographic directions [5]. Sometimes, such nanoelectronics applications require nanoscale devices in intricate geometries to accomplish the desired functionalities [6]. One way to meet this demand is to fabricate metamaterials [6,7] self-assembled structures or some exotic microstructures consisting of well-organized periodically distributed distinct phases/component, possessing desired functionality [8] (Figures 1.1-1.5, and 1.10-1.13). The fabrication of such functional materials with nanometric basic building blocks comes under the nanoarchitectonics regime [9], e.g., supramolecular chemistry [10], self-assembly/self-organization to produce advanced nanoelectronics components [9]. Such well-organized microstructures are achievable not only via some modern and hard-to-scale up techniques such as e-beam lithography [11], templated chemical vapour deposition [5] and pulsed laser deposition [12] but also with various classical phase separation routes, such as spinodal decomposition [13], pearlitic transformation, order-disorder transformation [14,15], martensitic transformation [16], intergrowth [17], and 3D self-assembled chessboard (CB)-like microstructural evolution [15,18–20] etc. However, most of them are potent to produce lamellae, well-organized precipitates and nanowires [5], which have been well understood and reported. Amongst all the techniques mentioned above, CB-like microstructural evolution is found to be the most suitable one for the given applications due to its unique potency to produce 3D well-organized interlacing of two chemically separable and structurally distinct cuboidal nanodomains, possessing functionality of the desired properties [8]. Top of the all, the CB-like microstructure domains are reportedly pretty homogeneous in terms of size, shape and compositional distribution [8,21]. Physical properties of a multiphase material not only depend on the structure of ingredient phases but also on their shape, size and morphological distribution [5,22,23]. The morphological features in such microstructures, mainly the size of the nanodomains and their relative concentrations, can be tuned by heat treatment and the stoichiometric ratio of the precursors. The mechanisms of the CB-like microstructural evolution have been a subject of extensive theoretical and experimental research in recent years [24,25]. Once the mechanism is established precisely for a specific crystal system,

the same parametric correlations can be extended for developing other CB-like microstructures based on that crystal system but for different applications.

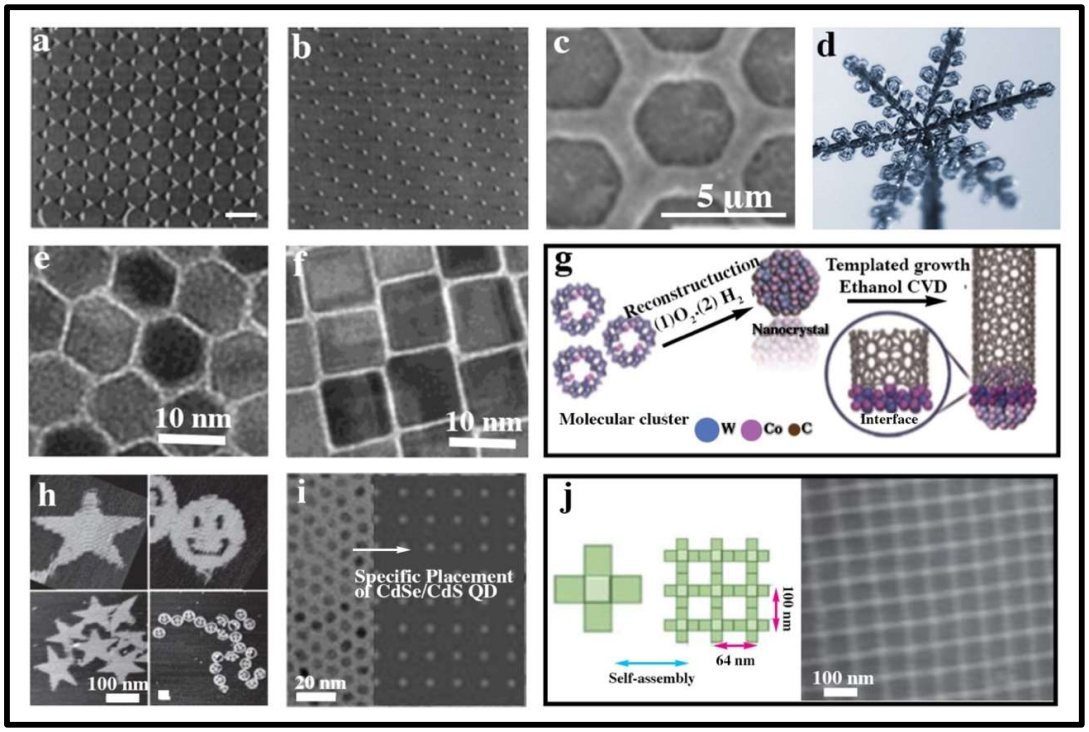

Figure 1.1: *A variety of patterned nanostructures obtained by (a, b) array of triangular metal dots obtained after removal of a single layer nanosphere mask and double layer nanosphere mask by multiple-patterning nanosphere lithography followed by oxygen plasma etching, respectively [26] (c) SEM micrograph showing the self-assembly of nanospheres inside the templates to form multiple layers [27](d) self-assembly of water molecules in the form of snowflake (e, f) TEM images of the as synthesized polyhedron-shaped and cuboid-shaped $MnFe_2O_4$ nanoparticles synthesized through shape-induced texturing of the particles through self-assembly, respectively [22](g) CNT growth on SiO_2/Si substrates via ethanol CVD, here W_6Co_7 alloy nanoparticles help in controlling chirality by lipid supramolecular self-assembly process [28] (h) fabrication of 3D building blocks in desired shapes using the DNA-directed self-assembly [29] (i) TEM image of the CdSe/CdS quantum dots (QD) suspended in octane (left), patterned placement of QD through e-beam patterning (right) [30] (j) Schematic of DNA origami nanostructures formed via the lipid-bilayer-assisted self-assembly technique, AFM image of the lattice [11,31].*

In this study, an attempt has been made to elucidate the mechanism of CB-like microstructural evolution in an essential class of nanocomposites developed for High-

Density Magnetic Storage Devices [8,25], and All Solid State Li-ion Batteries (ASSLBs) [32,33]. Despite the fact that various investigations have been made so far, this problem still has scope for further elucidation. Before going into the intricacy of self-assembled well-organised CB-like microstructure and its evolution mechanism, a brief knowledge of self-assembled structure, metamaterials, architectonics and phase separation is required.

1.1 Self-assembly

Self-assembly (SA) is a natural phenomenon by which a system arranges its basic components, e.g., colloids [34], macroscopic/microscopic particles, molecules or domains [35], into a well-organised functional structures by interaction among them (Figure 1.1). These interactions between the basic components may happen directly (repulsion/attraction) or through any environment (magnetic field/flux, hydrostatic field, electric field/flux, magnetohydrodynamic, etc.). These interactions can originate due to variety of forces/bonds, e.g. coulomb interactions, electrostatic interaction, van der Waals (vdW) forces, π-π bonds, capillary forces, entropic forces, and hydrogen bonds. In general, these local interactions try to interlace basic components/building blocks in a minimum energy configuration [36,37]. Minimum energy configuration brings the system closer to the equilibrium and simultaneously emanates a unique patterning ability in the system, which makes it potent to design materials for nanoarchitectonics [9]. In addition to that, significant progress in the chemicals and materials science synthesis techniques and instrumentations, facilitates precise control over manipulation of these interactions, which helps in designing intricately patterned microstructures. These advanced features make SAs much more reliable in designing patterned microstructures than most of the advanced manipulation techniques such as atomic traps, optical tweezers, scanning tunnelling microscopy (STM) [38] and atom force microscopy (AFM) [11,20].

1.1.1 Classification of self-assembled structures

Self-assembly (SA) can be classified as either static/equilibrium (SSA) or dynamic/non-equilibrium (DySA) based on their ability to remain/attain the minimum energy configuration in the given thermodynamic conditions (Figure 1.2). However, it is not necessary that the whole system can achieve equilibrium simultaneously. Depending on circumstances, a system can achieve local or global equilibrium by lowering its total free energy in numerous ways [25]. Hence, it is the type of system and the type of interactions

that ultimately decides as to which route it will follow (SSA or DySA) to reach a stable configuration.

1.1.1.1 Static/Equilibrium self-assembly (SSA)

Any SA system is considered as SSA, if it acquires a fixed organization of the basic components that does not reconfigure further under the influence of regulating external conditions, i.e., thermodynamic conditions, energy/field supply/flux, etc. In this condition, SA refers to a stable equilibrium structure, and no systematic energy will be flowing (do not dissipate energy) through it. In SSA, the formation of the organized microstructure may demand energy in single or multiple forms (interaction forces/interactions). SSA system achieves a stable configuration by counterbalancing all the interactions, and does not alter further under the influence of external energy/interaction/field (Figure 1.2). The common interactions between the particles or particle and surface are electrostatic (attractive/repulsive), vdW (attractive), dipole-dipole (attractive/repulsive), hydrophobic (attractive), aromatic (π-π) (attractive) and capillary (attractive/repulsive), gravity and flow/flux/field, etc. [20]. In SSAs the equilibrium can be obtained by achieving maximum entropy (local or global). The variation in the Gibbs free energy during the process ($\Delta G = \Delta H - T\Delta S$ (at constant temperature (T), pressure (P), and number of atoms/motifs (N)), defines the spontaneity of the reaction [38]. The process will be spontaneous if $\Delta G < 0$. Similarly, for constant temperature (T), Volume (V) and number of atoms (N), if the change in Helmholtz free energy $\Delta F = \Delta U - T\Delta S$ is < 0, the process will be spontaneous [39]. These equations suggest that SA can be regulated with both enthalpic ΔH or $\Delta U < 0$, $\Delta S \approx 0$, and entropic effects (ΔH or $\Delta U \approx 0$, $\Delta S > 0$), or both [36].

1.1.1.2 Dynamic/non-equilibrium self-assembly (DySA)

DySA refers to a well-organized non-equilibrium assembly, which maintains order by a flow of energy, even if the system is far from equilibrium. DySA builds through a continuous energy flux that stabilizes a non-equilibrium system and changes its organizational patterns according to the external thermodynamic conditions (Figure 1.2).

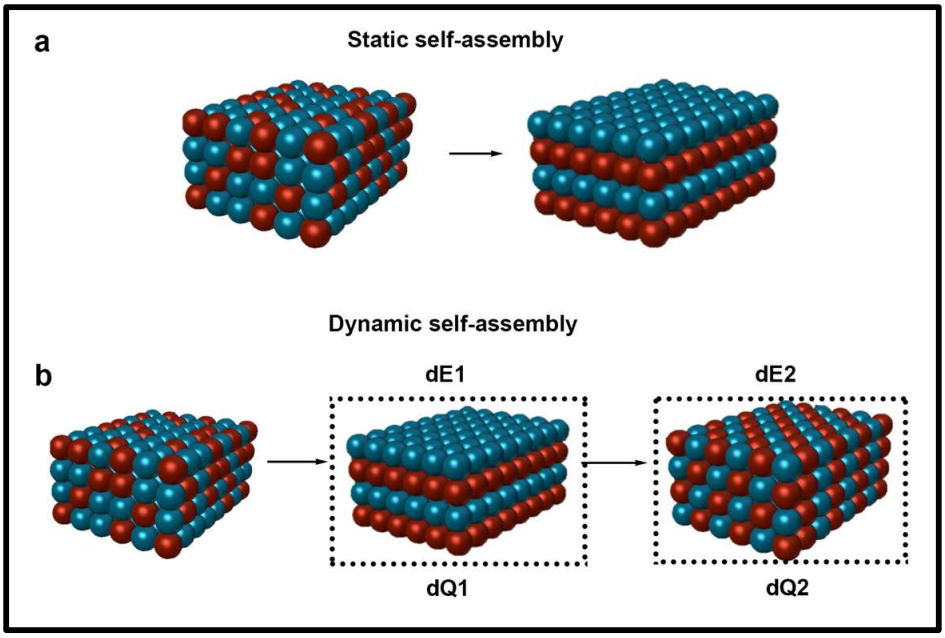

Figure 1.2: *Equilibrium/static (SSA) and non-equilibrium/dynamic (DySA) self-assemblies in a binary system. SSA, arranged basic building blocks in a "static" structure without any energy exchange through it. The arrangement does not change due to any thermodynamic variation. In DySA, a flux of energy in any form (here dE1) flows through the system that maintains the structure in any of its metastable states. These metastable states depend on the magnitude of flux, any manipulation in the energy/flux (dE1-dE2) may alter the arrangement to other suitable metastable state [36].*

A disordered collection of basic building blocks turns into a well-organized assembly, under the influence of energy input. As the energy flow regulates, the system acquires different configurations. DySA can be energy driven, entropy-driven, surface energy-driven (templated growth) [11] or field-directed (magnetic/electric) [36,40]. The DySA system disintegrates, when no energy is driving it. A DySA system only can attain the best ordering configuration when there are two or more competitive interactions counterbalancing each other's effect commensurately. If there are only repulsive forces in the system, the system will fall apart. On the other hand, if only attractive forces are acting in the system, it might be dynamically organized but not in the best possible configuration (closed packed). The 'competing' attractive and repulsive forces possibly introduce selectivity into the system and provide it with the best possible close-packed organization. The Design and synthesis of any DySA can be systematically controlled by external energy supply with various complementary interaction forces [36].

1.1.2 Applications of SA in nanoachitectonics

SA finds applications in various fields ranging from complex device fabrication [6] [41], electronic circuit, chip design [42], nanoarchitectonics [43], sensing, energy-harvesting [19,33], biomedical [20,44], and many more (Figure 1.3). Some SAs are already finding industrial applications. Alien Technologies have utilised fluidic self-assembly techniques to fabricate radio-frequency identification (RFID) tags based on shape recognition features. SA also finds application in energy storage technology, e.g., self-assembled monolayers for battery (Figure 1.3(b)) [45], 3D self-assembled battery [46]. In another case, IBM has harnessed the SA of trillions of nanometre-sized holes in computer chips (a few mm wide) to create exotic insulators capable of improving the efficiency and speed of transmission of the electric signal by 15% and 5%, respectively [42]. In addition, SA is also opening entirely new dimension of nanoarchitectonics that provides standard strategies for nanoelectronics design.

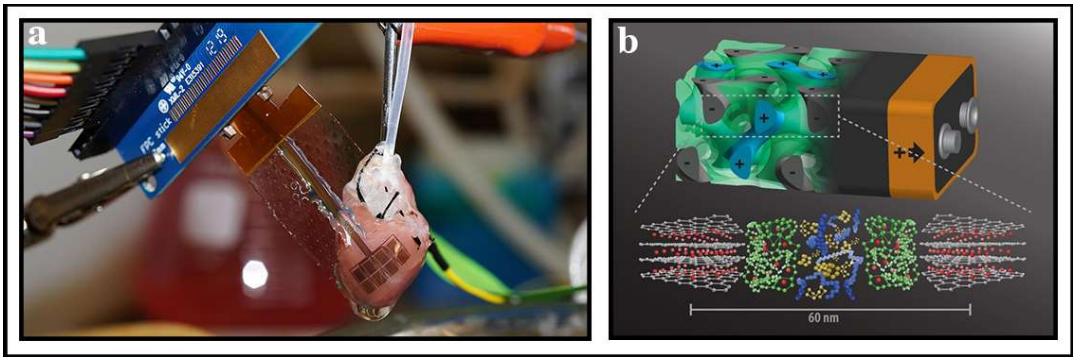

Figure 1.3 *(a) Designing Carbon-based bioelectronics devices such as tissue stimulator by utilising self-assembly for Parkinson's or cardiac problems [44]. (b)schematic representation of anode (grey), cathode (blue) and separator (green) with corresponding molecular structure of each layer in a 3D battery [46].*

The utilization of nanoarchitectonics in device design was first suggested by Health et.al. in 1999 (UCLA) [44]. On the other hand, DySA is still in its inception and can rationally tailor functional materials from variety of interactions at different length scales. Its ability to assemble elementary blocks of the systems in metastable states unlatch exciting possibilities to develop entirely new types of materials that can reconfigure themselves according to the external physical conditions. These flexibilities can provide a roadmap to

design responsive sensors, actuators, energy storage devices, and chemical amplifiers adapting to environmental conditions by reconfiguring their organisation. DySA can be considered the future of SA because it facilitates the designing of non-equilibrium systems that have the potential to design machines one step closer to living systems.

A well-organised patterning of the basic building blocks provides exotic physical properties that are not achievable in any naturally developed material. However, this kind of patterning is also possible from modern man engineered materials called 'metamaterials'(Figure 1.4). Hence, it is crucial first to establish a clear distinction between self-assembled materials and metamaterials.

1.2 Metamaterials (MM)

The word metamaterial is a combination of two words meta and materia; meta is derived from Greek meaning beyond, and materia is derived from Latin meaning matter [41]. The meaning is self-explanatory; a material shows properties that are not found in naturally occurring materials (Figures 1.4, and 1.5) [7]. The definition of metamaterials has been modified over time as its area of applications broadened. Studies of chiral materials by Jagdish Chandra Bose in 1898 can be considered as one of the early works on metamaterials [47]. He reported very first artificial composite material displaying optical activity in the microwave [7]. Although Victor Veselago first proposed the concept of metamaterials (negative refractive index materials) theoretically in year 1968 [48]. The very first report which clearly defines metamaterials was published in 2005. According to this report, a 'metamaterial' is defined very specifically as a 'composite medium', a periodic patterning of spaced nonmagnetic conducting split-ring-type resonators (SRR) and continuous wires. Further, in 2010 the definition got generalised as an arrangement of artificial elements, designed to achieve advantageous and unusual electromagnetic properties. Later in 2015, as many varieties of metamaterial came into light, the definition shifted to a more generalised term, 'artificial media', structured on a size scale smaller than the wavelength of external stimuli.

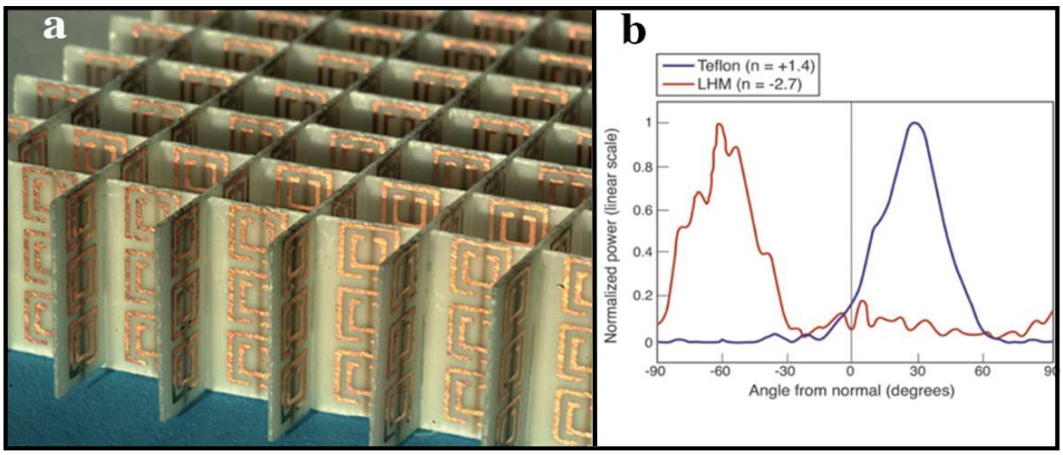

Figure 1.4: ***(a)*** *A metamaterial possessing negative index fabricated by SRRs and wires deposited lithographically on the opposite sides of a standard circuit board.* ***(b)*** *a graph obtained by Snell's law experiment shows power detected as a function of angle performed on a negative index sample and a Teflon sample* [3].

However, these days, the field of applications of metamaterials has crossed the barriers of electromagnetics and has become the only solution for most of the unnatural wave phenomena. Metamaterials are artificial composite materials, fabricated of two or more human engineered constituent components/basic building blocks, which exhibit exotic properties that cannot be derived from individual constituent components or any naturally occurring material.

However, metamaterials resemble self-assembled structures in terms of repeating arrangement of basic building blocks, their basic building blocks (Figure 1.4(a)) are bit different form SA's basic components as shown in Figure 1.1(e, f) and Figure 1.10-1.13. The properties of MM are dependent on the composition, crystal structure, shape, size, arrangement, and orientation of elementary building blocks (Figure 1.5). Top of the all, their patterning fashion is the prime factor that makes them potent to achieve properties that are impossible through conventional materials [7]. Their reported applications primarily include manipulating electromagnetic waves such as aerospace communications, remote sensing, energy harvesting [49], electromagnetic lenses, ultrasonic sensors for intelligent medical devices, shielding structures from earthquakes, etc. [3,7].

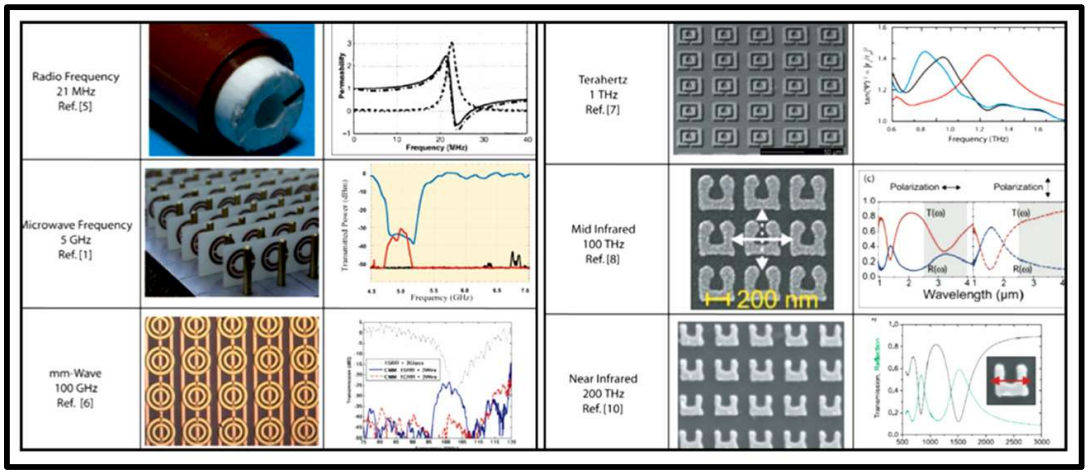

Figure 1.5: *Various type MM devices developed for a range of frequency from radio to near optical frequencies. Frequency ranges are mentioned in left column, middle column shows photo of corresponding MM, and third column summarises their performance details [3].*

1.3 Self-assembled materials Vs Metamaterials

Self-assembly (SA) is the autonomous organization of components/basic building blocks into patterns or well-organised structures without human intervention [7,9,11]. In contrast, metamaterials come into realization after human intervention and require various engineering approaches, i.e., laser lithography, templated growth [11], DNA/RNA origami [50]), manipulative microscopy (STEM or AFM) etc. [20] (Figure 1.1). In SA, the organization of these elementary building blocks depends on various factors, e.g., external/internal thermodynamics, interaction forces, dispersive media. Most of these factors can be applied to 1D, 2D and 3D self-assembled materials. Whereas these factors are not applicable for metamaterials, only mutual compatibility and positioning of components matters to get the desired output [7,49]. SA can be classified based on the modifiability of the patterning organization, whereas no such reconfiguration concept works for MM. However, materials with such patterned structures can be fabricated by various above-mentioned self-assemblies. However, it is hard to scale up MM engineering techniques.

In some metallic and ceramic systems, a critically controlled phase separation process can also develop similar well-organised patterned structures (Figures 1.9-1.13). Phase separation processes such as spinodal decomposition and preferential precipitation [51],

charge ordering [52], magnetic ordering etc., in combination with self-assembly, may facilitate the genesis of various intriguing patterned microstructures [18,53].

1.4 Theory of phase separation

Phase separation is the process by which an unstable or metastable material system minimises its total free energy to attain/proceed towards the equilibrium [25]. Generally, a material system is considered thermodynamically unstable when it has excess free energy $\Delta G = \Delta H - T\Delta S$, $\Delta G < 0$ between the parent and the product. The ΔG can be defined in terms of configurational entropy, enthalpy, lattice strain, surface tension, etc. [21,54]. However, a system also may become unstable under other forms of energy/fields, e.g., external magnetic fields, electrical fields, and electromagnetic radiation. Hence, chemical phase separation is not the only way by which a system can minimise its total free energy. Indeed, there are many other ways for a system to attain the ultimate equilibrium. An unstable/metastable system may opt for other phase transformation routes by which it can minimize the excess energy, such as electronic phase separation [55,56], structural phase separation [57,58] magnetic phase separation etc [59].

1.4.1 Chemical phase separation

Phase separation is a widely used term which refers to the evolution/formation/ decomposition of different phases within a homogeneous solid solution or matrix. For instance, a system consists of two different atoms A and B, mixed in a fixed stoichiometric ratio, is exposed to some given thermodynamic condition. Naturally, for these given thermodynamic conditions the system will always try to arrange A and B atoms in such a way so that it can minimize its overall energy. Both the atoms, depending on their physical identity, i.e., atomic size, electronic configuration, etc., can arrange themselves in several stoichiometries, shapes (morphology) and stacking arrangements (crystal structure). These physically distinct and chemically separable regions are called phases. Their physical conditions define how far these phases are from the ideal equilibrium. The formation of distinct phases of same constituent atoms not only depends on thermodynamic condition but also depends on various other factors defined by many established rules, i.e., Hume-Rothery [60], Pauling principles, lattice gas model [61], Density function theory (DFT) [62], crystal field theory (CFT) [63,64], and molecular orbital theory. CFT combined with molecular orbital theory (MOT) provide more realistic and complex ligand field theory (LFT), which gives insight about chemical bonding in complex materials.

To keep it simple, in this section we are mainly focused on two aspects of phase separation, chemical phase separation and its thermodynamic constraints. In a solid solution, chemical phase separation depends on various factors, e.g., solid solubility of elements/phases, interaction parameter, nature of bonding, chemical potential, etc. In general, solid solubility decreases with decreasing temperature, and a miscibility gap forms between a solute-rich phase and a solvent rich phase resulting in chemical potential variation. Difference in chemical potential of the phases derives chemical phase separation. Phase separation occurs in a similar way as heat transfers until temperature gradient exists, volume changes until the pressure becomes equal, atomic diffusion happens so long chemical potential exists.

1.4.1.1 Spinodal decomposition

Spinodal decomposition was first noticed by Bradly in the early 1940s [65]. He noticed it in the form of side-peaks in XRD patterns of quenched Cu-Ni-Fe alloy. Later, Daniel and Lipson led this investigation [66]. They related these side-peaks with a periodic composition modulation in specific <100> directions. Later, Mats Hillert came up with a proper explanation of spinodal decomposition in famous Cahn-Hilliard model in his 1955 Doctoral Dissertation at MIT. If the composition of any system falls within the miscibility gap between X_1 and X_2, it becomes thermodynamically unstable (Figure 1.6). Since phase separation is energetically favourable in this range, outside the miscibility gap, the system remains in equilibrium irrespective of its composition and temperature. For a system whose composition falls in the miscibility gap, Gibbs proposed two-phase transformation routes through which it may lower its free energy. First, if a system falls under the chemical spinodal curve with a linear instability ($\frac{d^2G}{dx^2} < 0$) which is small in degree and larger in extent (slight composition fluctuation spread over a larger area), these fluctuations will grow spontaneously and trigger the spinodal decomposition homogeneously in order to neutralise the chemical potential difference. However, in some specific conditions, the phase separation can follow the nucleation and growth route, even in the spinodal region. Second, for the composition of an unstable system with nonlinear instability ($\frac{d^2G}{dx^2} > 0$), i.e., larger in degree and minor in extent (significant composition fluctuation spread in a small area), it falls in the binodal region (miscibility gap - area under the spinodal curve, Figure 1.6 (a)). This condition follows the nucleation and growth route for phase separation. Consider a homogeneous alloy with composition X has gone under a sinusoidal composition fluctuation of ΔX amplitude and wavelength λ.

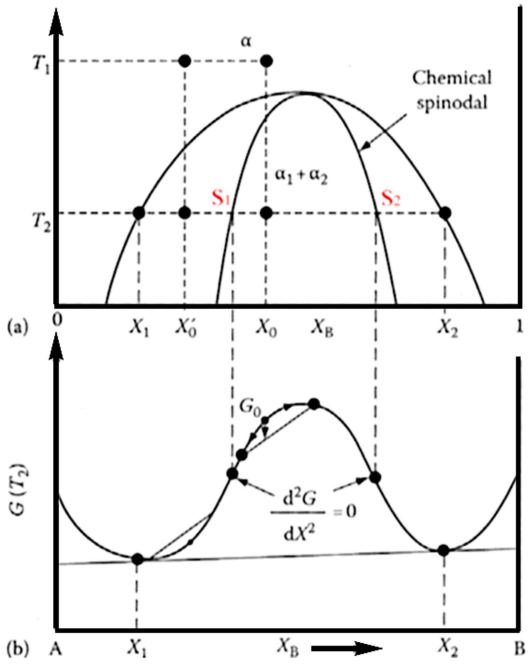

Figure 1.6: *Schematic representation of spinodal decomposition (a) spinodal and binodal curves (b) Gibbs free energy Vs. Composition graph showing point of inflection and equilibrium composition at X_1 and X_2 [54,67].*

A phase separation through spinodal decomposition brings overall free energy down that results in finely dispersed phases with a specific wavelength of two distinct compositions but similar crystal structures. A wavelength of compositional modulation can only sustain when it is larger than the critical wavelength **λ**c, all wavelengths shorter than the critical value die out as the decomposition proceeds to decrease the total Gibbs energy [68].

$$\Delta G = \frac{1}{2}\frac{d^2G}{dx^2}(\Delta X)^2 + K\left(\frac{\Delta X}{\lambda}\right)^2 + \eta^2(\Delta X)^2 E' V_m \quad \ldots(i)$$

$$\Delta G < 0, \lambda > \lambda_c = [-2K/(\frac{d^2G}{dx^2} + 2\eta^2 E' V_m)]^{1/2} \quad \ldots(ii)$$

In equation (i) first term corresponds to the chemical energy contribution. In the same equation second term denotes interfacial energy contribution. Third term includes interfacial strain and η is defined as η = (da/dX)/a. In fact, creation of two regions with certain composition gradient consume extra free energy of the system. This includes an interfacial energy or surface tension, ΔGγ, that depends on the chemical composition gradient across the interface; and is called gradient energy. Where λ is the wavelength of

composition fluctuations, E' is elastic modulus $E' = E/(1-\nu)$, ν passion ratio Vm stands for molar volume and K is a proportionality constant that depends on the bonding energy difference of the pair of similar and dissimilar atoms. The decomposition of a parent phase results in product phases with different compositions. These product phases will definitely have difference in lattice parameter. This lattice parameter mismatch/coherency strains at the interface will contribute to the total energy of the system.

1.4.1.2 Nucleation and growth

Nucleation and growth is another way to minimise the total free energy of a metastable system. When the composition of a system falls in the miscibility gap (area between spinodal and binodal curves), it becomes metastable (Figure 1.6). From the metastable condition, nucleation is the most suitable way to reach equilibrium. Volmer, Becker and D¨oring have contributed the earliest work in the classical nucleation theory [69]. Since nucleation is a nonlinear instability, it requires an immediate formation of a low-energy phase to reduce the free energy up to a critical limit locally.

$$\Delta G = \frac{4}{3}\pi r^3 \Delta G_{chem} + \frac{4}{3}\pi r^3 \Delta G_{chem} + 4\pi r^2 \sigma_2^x \gamma$$

Where $\Delta G_{chem} = GX_2V - Gc_*V$, is the chemical free energy change and G_{strain} is the strain energy per unit volume associated with the creation of X_2. Here GX_2V and Gc_*V represent the free energy per unit volume of precipitate with critical size and matrix, respectively [70,71].

1.4.1.3 Pseudospinodal decomposition

Pseudospinodal decomposition has most of the signature features of the spinodal decomposition. However, there are some deviations, i.e. the crystal structure of product phases, nature of their interface, and their microstructural arrangement. In spinodal decomposition, both the product phases possess the same crystal structure as their parental phases. Whereas in pseudospinodal decomposition single/both product phases may deviate from the parental structure. However, in both spinodal and pseudospinodal decomposition, compositional separation happens by uphill gradual diffusion/separation of both the product phases. In spinodal decomposition the product phases are only distinguished by composition, product phases of pseudospinodal decomposition are also distinguished by symmetry determined long-range order parameter (SLRO) [21,25].

1.4.2 Order-disorder transformation

In a solid, ordering may be defined as the tendency of its atoms to surround itself with unlike atoms. Often metallic systems show the tendency to have such kind of arrangements at low temperatures. One of the earliest observations of ordered structures was made by Tammann et al. [72,73]. On the basis of some chemical experiments (without X-ray evidence), they observed that when a suitably conditioned Cu-Au alloy (Cu >50 at%) was attacked by nitric acid, only Cu atoms were affected by nitric acid and dissolved, but none of the Au atoms. However, the nitric acid did not affect the Cu-Au alloy containing Cu <50 at%. The ordering behaviour of any system can be classified based on its length scale, charge ordering, spin ordering and density ordering, etc. Ordering behaviours ultimately show their consequences on physical properties. However, the ordering tendency of atoms depends on various factors, e.g., atomic size, electronegativity, spin, charge, orbital, structural degrees of freedom and thermodynamic conditions [73]. These ordered structures produce many intriguing microstructural features, i.e., anti-phase boundaries (APB) and interphase boundaries (IPB), generating remarkable physical properties [74]. In a bulk material, the ordering can be triggered at multiple sites and may create coherent interfaces in the systems where the stacking sequence of two adjacent regions is reversed. If two same phases with inversed ordering share a coherent interface, it is called APB (Figure 1.7). Ordering in the atomic arrangement can be understood by the Greedy-lattice-gas model, which is explained in the following section. Interphase boundaries (IPBs) is a special situation in which two phases share a boundary when at least one of them is ordered or both of them are disordered. In anti-phase boundaries, the ordering behaviour changes across the boundary within the same phase [74]. It is associated with a translation vector within the lattice, which is reflected in the diffraction pattern or in the direct structure image of the lattice. Depending on the extent of ordering, it can be classified into different categories

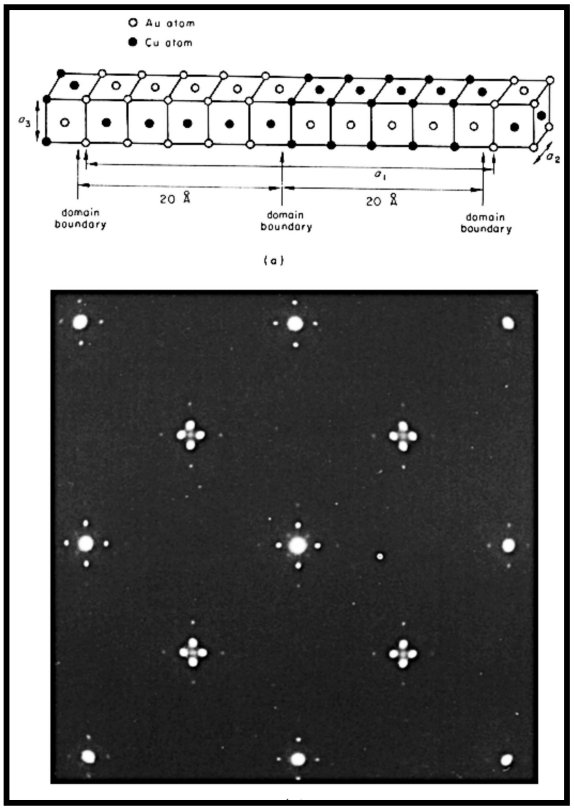

Figure 1.7: *Schematic representation of two APB in Au-Cu alloy (a) corresponding electron diffraction pattern along [001] zone axis showing satellite spots [75].*

(a) Short range order

The degree of randomisation of a system depends on many factors such as the nature of bonding, thermodynamic conditions, size of atoms, external fields etc. However, in metallic systems it is primarily governed by the nature of bonding and temperature. If the constituent atoms are prone to be surrounded by unlike atoms, then the situation is favourable for ordering of constituent atoms to minimise the overall free energy. At higher temperatures, such tendency may be diminished and the system may again migrate to disordered state. If the system prefers to surround a particular kind of atom by unlike atoms up to the third-nearest neighbour, the magnitude of the randomness would drop rapidly. Such arrangement is termed as short-range order.

(b) Long range order

If the ordering tendency is higher or the temperature is low enough, atoms or molecules will try to minimise the degree of randomness. If there is a site-specificity between the atoms, then atomic occupancy occurs in specific sites all through the lattice. It can be mathematically correlated to understand the extent of order. This situation is known as long range order.

1.4.2.1 Charge ordering (CO)

Verwey coined the idea of charge ordering in 1939 [56,76], where he observed a significant increase in electrical resistivity in a magnetite (Fe_3O_4) sample at low temperature (120K), known as Verwey transition. CO is a phase transition process that occurs primarily in strongly organized materials such as transition metal oxides, rare earth-transition metal oxide or organic conductors. A strong interaction between the electrons promotes charge localization on particular sites leading to ordered structures. This charge ordering transition breaks crystal symmetry in an organized way that generates new physical properties, e.g., ferroelectricity, ferromagnetism, anti-ferromagnetism etc. CO transition can occur in multidimensions and can appear in different patterns ranging from vertical to horizontal stripes to a checkerboard-like pattern. Recently, this charge-ordered structure of magnetite was solved by Paul Attfield et al. in 2011[56].

CO in transition metal-based ceramic systems has become a popular area of research due to their exceptional ability to show multiple oxidation states, i.e. mixed valent manganite [59], rare-earth-based perovskites [77]. These materials show intriguing physical properties due to phase transition, which occurs in these materials as a consequence of competition between, e.g., super-exchange, double exchange, and electron-lattice couplings [78]. In addition to electron-lattice coupling, double-exchange, and super-exchange, Jahn-Teller distortion also plays a vital role in the manganite physics [59][79]. Due to the complexity of these exotic phenomenon, it is difficult to identify the role of individual phenomenon in phase transitions in such materials.

1.4.2.2 Magnetic ordering (MO)

Magnetic ordering is a much more complex phenomenon than charge ordering. In magnetic ordering, it is not only atomic ordering that changes the overall magnetic behaviour of the material, spin direction also plays a vital role.

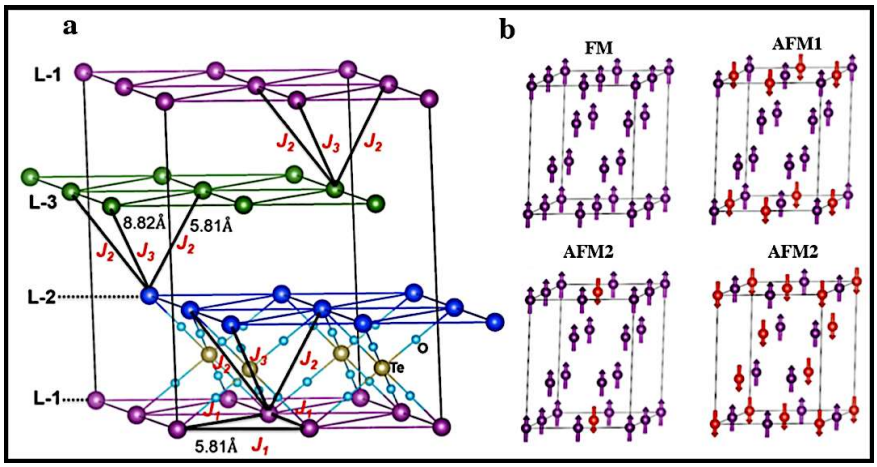

Figure 1.8: *The exchange interaction for the Mn spins in layered double perovskite Ba_2MnTeO_6 (a) J_1 represents an in-plane exchange interaction with nearest neighbour. Whereas J_2 and J_3 are out-of-plane interactions with nearest and next-nearest neighbour.(b) in such compounds these interaction may produce four types of magnetic interactions, e.g., FM (ferromagnetic), AFM1 (anti ferromagnetic), AFM2, and AFM3 [80].*

Changing spin directions of neighbouring atoms might vary interaction energy of the atoms that influences the bonding nature of constituents. Spin interactions between the neighbouring atoms may introduce three pairs of interaction energies, i.e., spin-up-spin-up, spin-down-spin-down and spin-up-spin-down (Figure 1.8(b)). For instance, the magnetization behaviour of iron changes on heating above the Curie temperature. Due to ferromagnetic-paramagnetic transition, iron losses its magnetic order and demagnetizes [79]. Short range and long-range ordering have been seen in double perovskite based Ba_2MnTeO_6 (Figure 1.8).

1.4.3 Structural phase separation

Some unstable systems reduce their free energy by polymorphic phase transformation where the composition of the product phases remains almost constant, whereas their structure changes to two distinct but relatable structures with the parent phase. For instance, structural phase separation in $K_{0.8}Fe_{1.6+x}Se_2$ Superconductors (Figure 1.9), results in two coexisted structural phases, antiferromagnetic phase $K_{0.8}Fe_{1.6}Se_2$ having modulating vector

q_1 = 1/5[3a* + b*], and another superconducting phase $K_yFe_2Se_2$, modulating vector q_2 = 1/2[a* + b] [51].

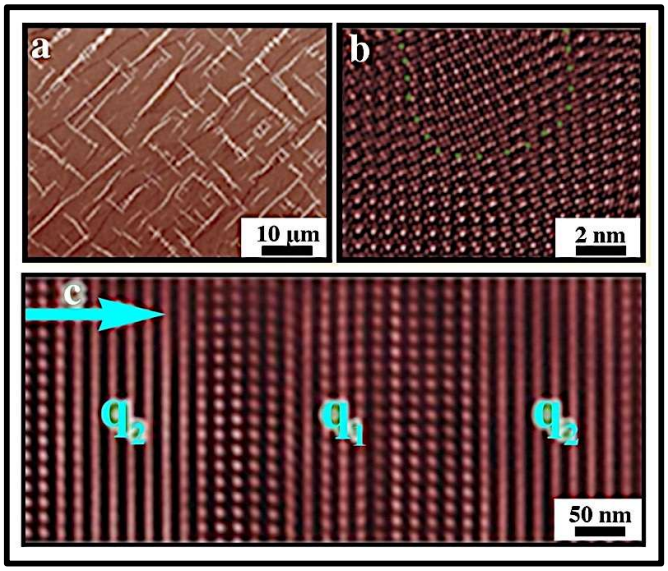

Figure 1.9: *SEM images of $K_{0.8}Fe_{1.6+x}Se_2$ superconducting sample showing presence of two phases as stripe-like patterns having interfaces along [110] and* $[1\bar{1}0]$ *directions. (b) phase contrast HR TEM image illustrating phase separated domains at nanoscale. (c) Alternative appearance of the $K_{0.8}Fe_{1.6}Se_2$ and $K_yFe_2Se_2$ phases [51].*

1.4.4 Electronic phase separation

Electronic phase separation is the phenomenon that produces inhomogeneous region in terms of the electronic/magnetic properties without making any observable distinction in the composition. In general, it occurs in multinary complex materials, where the interplay of orbital, spin, charge, lattice parameter, and degrees of freedom, produces dissimilarity in the electronic configuration in specific directions/portion of system [20]. These dissimilarities cause the genesis of distinct electronic/magnetic properties. These coexisting states can form at various length scales (macroscopic/microscopic) depending on the abovementioned factors and thermodynamic conditions (mostly at low temperatures) [81]. Electronic phase separation may produce contrasting properties like metallic-insulating, magnetic-nonmagnetic, colossal magnetoresistance, thermoelectric, etc. Amongst all, colossal magnetoresistance is an important effect of electronic phase separation. Here the magneto-resistive response increases with decreasing curie

temperature (T_C). For instance, in manganite perovskite, i.e., (La, Pr, Ca)MnO_3 different size of rare earth metals modifies local structural parameters, i.e. bond distance and angles. In this case, Mn-O bond distance and Mn–O–Mn bond angle gets modified that influence charge hopping between Mn ions, which leads to two coexisting and competing regions of different magnetic properties at the sub-μm-scale. One is ferromagnetic (FM) metallic phase, and another is a CE-type (charge exchange) charge-ordered (CO) phase [79]. These two phases coexist without noticeable compositional variations, indicating that this phase coexistence does not result from chemical phase separation [81,82].

1.5 History of self-assembled CB microstructures

3D self-assembled CB-like microstructures are reported in both metallic and ceramic systems. An extensive literature survey suggests that the evolution of the CB-like microstructures is system dependent and follows different phase transformation routes. CB-like microstructures were first reported in metallic systems, i.e., Cu-Au (Guymont et al.1982 [53,83] and Johannson et al.1936 [53]), Co-Pt (Leroux et al.,1991 [53] and Khachatuyan et al. in 1998 [15]). In metallic systems, order-disorder phase transformation ($Al \rightarrow Ll_2 \rightarrow L1_0 + Ll_2$) was found as a route for the evolution of checkerboard microstructures [53]. CB-like microstructures are also reported in ceramic systems, i.e., $CoFeMnO_4$ [8], $Mg(MnFe)O_4$ [1], $ZnMnGaO_4$ [4] spinels, and (LnLi)TiO_3 (Ln= Nd, Pr, La) perovskites systems [19,33,84]. It is not easy to figure out as to who reported CB evolution in ceramics for the first time. To the best knowledge of authors, Inaguma et al. in 1993 [85], and Garcia et al. in 1995 [32] have reported this phenomenon in (LnLi)TiO_3 (Ln= Nd, Pr, La) based perovskites, contemporarily. They concluded that in majority of the perovskites CB-like microstructure evolves due to the tilting of the BO_6 octahedra, a consequence of aliovatent cationic substitution at the A-site [19,33]. Whereas in majority of the manganite spinels J-T distortion works as the driving force, and a fast cubic to tetragonal transformation followed by a pseudospinodal decomposition gives birth to CB-like microstructure [8].

1.5.1 Proposed theory for self-assembled 3D chessboard microstructures

In contrast to metallic systems, there are only a few reports on the CB evolution mechanism in ceramics, and it is still sketchy and demands further elucidation. The evolution of such morphologies has been reported in metallic systems earlier than that of ceramics. Due to continuous efforts made so far by various research groups, the evolution mechanism of

metallic systems has been explained much more clearly. For metallic systems, it is well stabilised that a two-dimensional CB structure evolves due to the precipitation of the tetragonal phase in the cubic parent phase. Further, a relative orientation rearrangement driven by the strain-induced interaction develops between the coherent precipitates of the low-symmetry phase. Published reports on Co-Pt, AlNiCo, CuNiFe, TiNbAl, NiVX (X=Co, Nb, Fe), AuCu-Ag, AuCu-Pt, Fe-Co, $AuZu_4$, Ni-Al and $LiNdTiO_3$, $ZnGaMnO_4$, $Mg(ZnMn)O_4$, $CoFeMnO_4$ metallic and ceramic systems suggest that the evolution mechanism of CB in metallic systems is quite different from ceramic systems. However, the symmetry breaking phase formation is typical in both kinds of systems.

1.5.1.1 Tweed-like structure to CB-like microstructure

A.G. Khachaturya et al. first reported in 1998 that in a cubic matrix CB-like morphology evolves through a series of phase transformations [15]. Formation of a tweed-like structure, a tetragonal phase within a cubic matrix, has been identified as a primary phase transformation event (Figure 1.10(a)) [25]. Later this tweed-like nanostructure works as a template for CB-like microstructure growth, in which cubic and tetragonal domains grow with a continuous decomposition of two phases towards their equilibrium composition. Authors have explained the mechanism of CB-like evolution in a homogeneous cubic system with the help of thermodynamic theory of cascade decomposition.

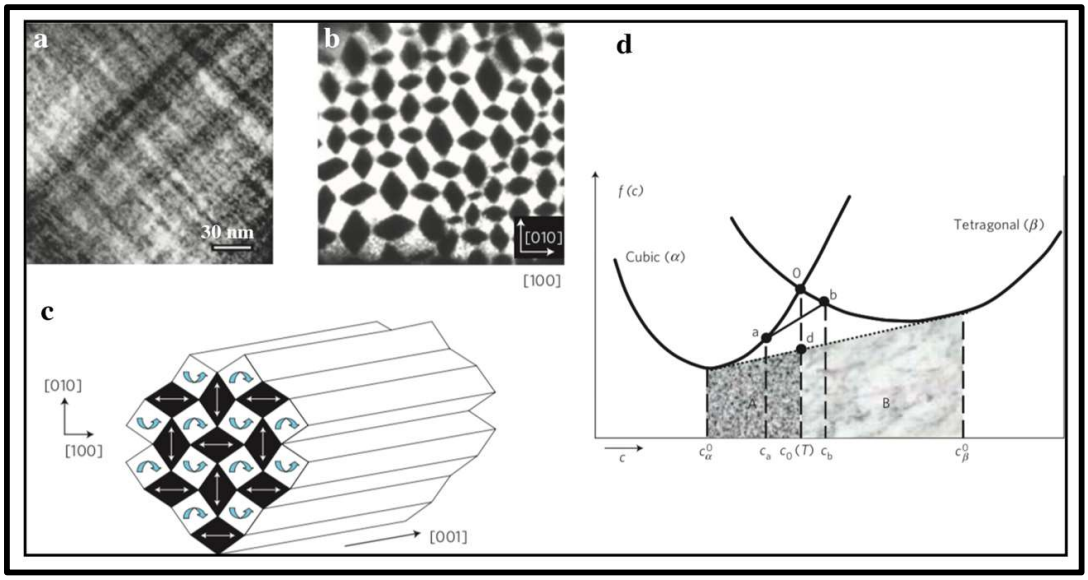

Figure 1.10: *(a) Bright field diffraction contrast image of precursor tweed that work as template for resultant chessboard structures shown in (b) along [100] (c) a 3D schematic chessboard nanowires, in which dark domains are representing tetragonal domains with two orientations (marked by arrow). In the (c) white domains are depicting cubic phase. (d) graph representing the variation of free-energy-versus-composition in A and B composition range for the tetragonal and cubic phases [25].*

Initially cubic system has a composition 'c' that decomposes into a mixture of equilibrium cubic (α) and tetragonal (β) phases with equilibrium compositions c_α^0, and c_β^0, respectively (Figure 1.10 (d)). To show the variation in the free energy with respect to temperature, author considered two separate composition ranges A and B spread between C = C_0(T) and both equilibrium composition c_α^0 and, c_β^0, respectively. C = C_0(T) is the composition where the free energy of both cubic and tetragonal phases is equal for a given composition. In the composition range 'A', free energy of the cubic phase α is lower than that of the tetragonal phase β at the same composition C_a, whereas, in range B at composition C_b, the situation is just opposite. Hence in composition range B, a fast cubic to tetragonal transformation is favourable, and a diffusionless cubic → tetragonal transformation can reduce the free energy without changing the composition. In this range, diffusionless crystal lattice rearrangement is the first leg of the equilibration. The second leg starts as a decomposition of this metastable tetragonal phase into a coherent mixture of cubic and tetragonal phases with a composition near to equilibrium c_α^0 and c_β^0. In this process, second leg takes longer

to complete because it involves a long-range diffusion. However, in range 'A' the situation is very much different, if the composition is very close to the mutual equilibrium composition C = C_0(T), the system will be far from equilibrium because its free energy exceeds the equilibrium value by a distance close to the length 0d (Figure 1.10 (d)). In this condition, phase separation is inescapable, and the precipitation of a tetragonal phase with a composition C_β falling in range 'A' can reduce the total free energy of the system compared to the initial matrix. Even if the newly precipitated phase C_β is far from the equilibrium composition of the tetragonal phase c_β^0. The compositional gap between the initial matrix and nucleated precipitates ($C_\beta - C_b$) can asymptotically disappear. The phase separation, in this case, will be called pseudospinodal decomposition. As this process involves long-range diffusion, it takes longer to reach equilibrium phases. However, the difference between pseudospinodal decomposition and true spinodal decomposition can be settled below a critical temperature [15][25].

1.5.1.2 J-T distortion assisted CB-like microstructural evolution

J-T distortion assisted evolution of CB-like microstructures is primarily reported in the transition metal-based spinel manganites (Figure 1.11(a-d)). Elements having d-orbital as their outer orbital show degeneracy if they have electrons in odd number, i.e., Mn^{3+}, Cu^{2+}. In this mechanism J-T distortion acts as symmetry breaking/driving force. The d-orbital of such cations degenerates into two groups of t_{2g}, and e_g orbitals dxy, dyz, dzx and dz^2, dx^2-z^2, respectively (Figure 1.11(e)). Amongst all transition metals, Mn^{+3} shows prominent degeneracy tendency. In spinel systems, once Mn^{+3} ion occupies B octahedral position, it coordinates with six oxygen atoms, which works as a weak legend and favours high spin filling of the unpaired electrons in one of the e_g subshells. The electronic configuration of Mn^{+3} (d^4) suggests an uneven filling of the e_g subshells, resulting in the repulsion of both the oxygen atoms in the Z direction. In these conditions, Mn^{+3} ion becomes J-T active that exhibits more than 10% elongation along Z-axis [001] in the original cubic structure.

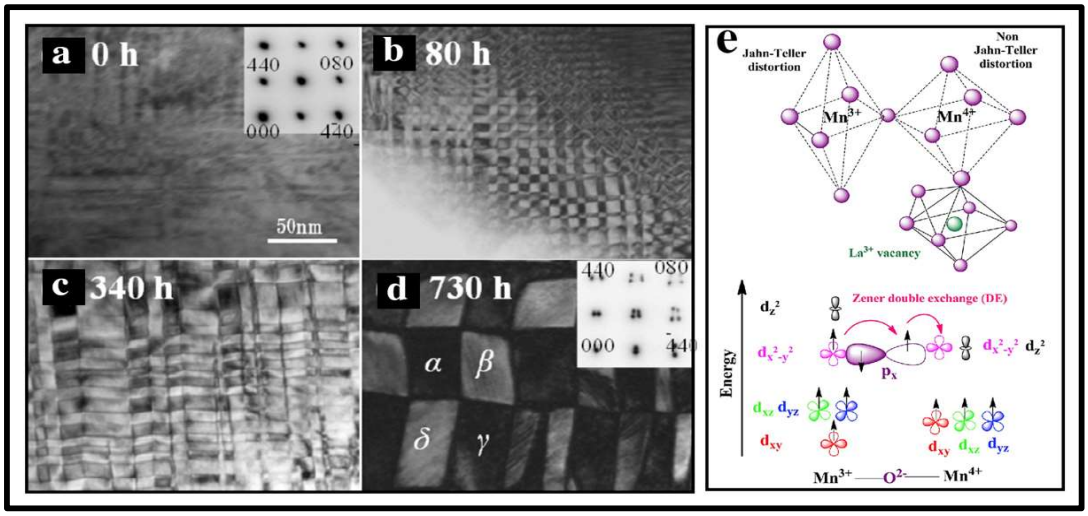

Figure 1.11: *Diffraction contrast images of $Co_{0.6}Fe_{0.9}Mn_{1.5}O_4$ sample, sintered at 1473 K for 20 hours followed by quenching and annealing at 648 K for (a) 0 hours, (b) 80 hours, (c) 340 hours and (d) 730 hours. Corresponding electron diffraction patterns are shown in the insets of (a), and (d). (e) Schematic representation of J-T distortion when Mn^{+3} is octahedrally coordinated with oxygen atoms causing splitting of d^4 in to degenerate subshells [35][86].*

Due to the increase in the Mn-O bond length in the Z direction, a complementary reduction in the remaining four Mn-O bond lengths will be observed [79]. The diffusion of more and more J-T active Mn^{+3} ions introduces the anisotropy in already unstable cubic phase. For any unstable system, spinodal decomposition is the best possible route to minimize its free energy. This cubic matrix would turn into J-T active and J-T inactive regions. Ultimately, two phases with different Mn concentration separate out in a well-organized CB-like microstructure. The misfit in the lattice parameters of Mn-rich and Mn-poor phases introduces solid body rotation to minimize the interfacial strain [8].

1.5.1.3 Order-disorder assisted CB-like microstructure

The evolution of CB-like microstructure by order-disorder transformation also has been reported. Such microstructural evolutions are predominantly reported in metallic systems, i.e., Cu-Au, Pt-Fe, Pt-Mn, Pt-Ni, and Pt-Co [53]. In this case ordering works as a symmetry breaking transformation. Although ordering reduces the symmetry of the underlying lattice, it brings down the overall free energy of the system. Ordering tendency becomes even more prominent at low temperatures. In most systems mentioned above, A and B atoms occupy

specific sites at lower temperatures. For AB_3 stoichiometry a cubic $L1_2$ type structures, and for AB stoichiometry a tetragonal $L1_0$ type structures are reported as simplest ordered structures. The coexistence of these two ordered phases produces intriguing microstructures, where transformation/separation of the secondary tetragonal phase from the cubic parent matrix could produce the two-dimensional CB structure. This CB evolution is driven by strain-induced interactions between the coherent low-symmetry phases. Here a coherent strain derives the 3D self-assemblage of three orientation variants of $L1_0$+$L1_2$ phases through order-disorder (Figure 1.12(a)). These phase variants evolve as rhombus domains whose facets generally grow normal to their elastically soft directions. For instance, in Co-Pt, CB evolves as two coexisting domains of $L1_2$ ($CoPt_3$,) and $L1_0$, (CoPt) phases, respectively. In an equiatomic mixture of Co-Pt a disordered phase (A1) forms at high temperature.

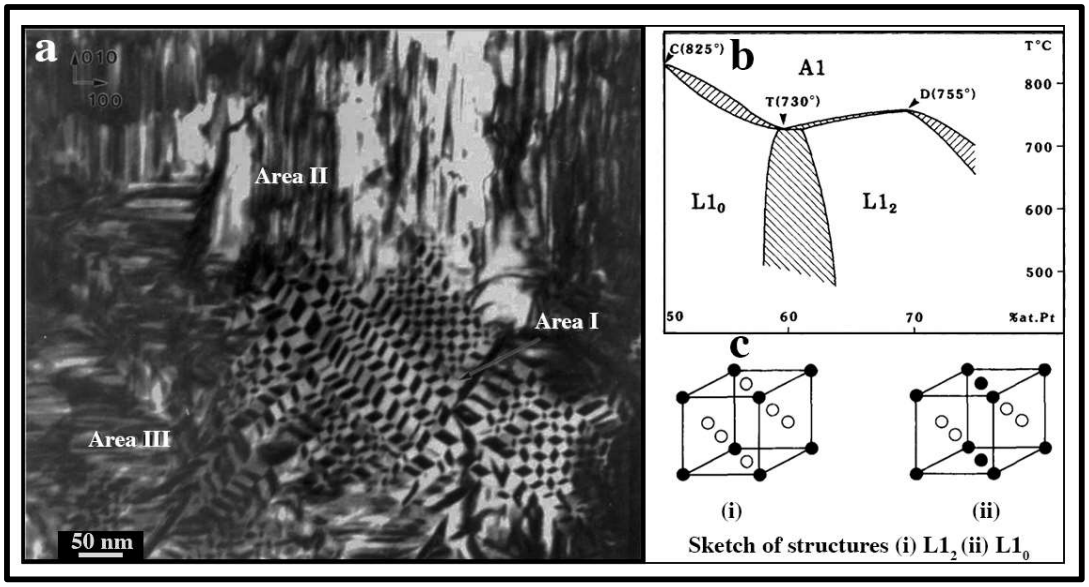

Figure 1.12: *DF image of typical $L1_0$+$L1_2$ microstructure oriented near [001], by selecting 110 spot, depicting the patchwork of I, II and III type areas. In area type I, only $L1_2$ domains are illuminated while, $L1_0$ domains are out of contrast. Similarly, other two orientation variant of $L1_0$+$L1_2$ patchworks (type II and type III) are denoted by arrows. (b) phase diagram of Co-Pt system in range 50-75 at.% pt. (c) schematic of $L1_2$ and $L1_0$ ordered structures, black and white atoms are representing A and B atoms [53].*

This high temperature disordered state Al can transform into two phase mixture through three different ways: (1) A1→Ll_0→$L1_0$+$L1_2$ (2) Al→Ll_2→$L1_0$+Ll_2 (3) Al→Ll_0+Ll_2

(Figure 1.12 (a)). Processes (1) and (2) involve two steps, where A1 acquires ordering in the first-step to $L1_0$ or Ll_2. The second step involves an interfacial wetting of the domain walls of the ordered structures ($L1_0$/Ll_2) formed during the first step. Whereas third way is quite different from the previous two, which involves a direct order-disorder transformation of two phases direct from a disordered phase (A1), a mixture $L1_0$+Ll_2 of ordered phases is formed in one step. A simultaneous appearance of phases Ll_0 and $L1_2$ within the disordered matrix forms an archetypal microstructure. Despite the route, in every case at the final stage, all the microstructures appear similar. However, it does not produce perfect square domains; regular tiling of domains resembles CB microstructure [53,57].

1.5.1.4 Octahedra tilting assisted CB-like microstructure

Octahedra tilt assisted mechanism has been reported to be responsible for CB-like microstructure evolution in $LiLnTiO_3$ (where Ln: Pr, Sr, La, Nd) perovskite systems (Figure 1.13) [87]. Here, Li and Ln ions occupied A-site. This aliovalent substitution of cations at the A-site introduces distortion in the cubic perovskite unit cell. To compensate this extra strain and bring down its total free energy, system prefers ordering of Li/Ln ions in 001 directions. Cationic ordering at A-site occurs even though the ratio deviates from 1:1. Guiton et al. reported CB-like microstructural evolution first in $(Ln_{2/3-x}Li_{3x})TiO_3$ perovskite system in 2007 [19,33,88]. Where he proposed that in $(Nd_{2/3-x}Li_{3x})TiO_3$ sample every second layer of Nd cations was replaced with a mixed layer of vacancy, Li-ion and Nd-ions, which doubles the lattice parameter in [001] direction. Ordering in [001] direction is considered as primary ordering. Secondary ordering occurs within the mixed cation layer, where Li-ion and Nd-ion swap their positions very strategically, that can be identified by satellite spots around the primary diffraction spots. This cooperative ordering of Li-ion in (001) along [010]/[100] direction minimizes coulombic repulsion between Li–Li and Li–Nd. In this case enthalpy of mixing goes positive side, which is essential for spinodal decomposition. This symmetry braking transition leads to the formation of CB-like complex two-dimensional array of twinned antiphase boundaries and compositional phase separation.

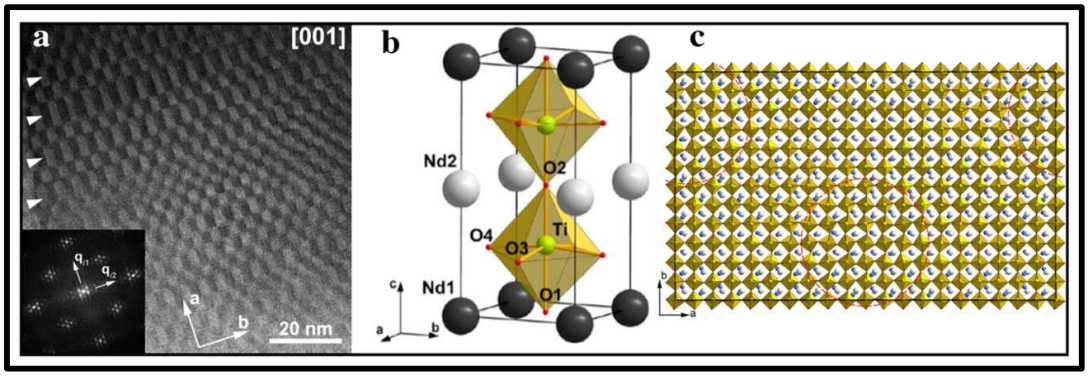

Figure 1.13: *(a) Phase contrast high resolution image of $Li_{0.15}Nd_{0.61}TiO_3$ sample sintered at 1250 °C followed by annealing (20 °C/hour) along [001] zone axis and corresponding fourier transformation (inset) (b) crystal structure of $LiNdTiO_3$ showing ordering in [001] direction. (c) schematic depicting alternative modulation of strain manifestation of tilt twinning of BO_6 octahedra [55].*

Later, Withers et al. [89] in their pioneering work suggested the involvement of strain modulation that manifests a periodic octahedral tilt twinning and partially occupied mixed layers containing lanthanide and lithium cations, and vacancies (Figure 1.13 (b)). However, through Z-contrast STEM imaging, they have showed the agreement with the earlier work of Guiton et al. In contradiction, Abakumov et al. have carried out a study on $Li_{3x}Nd_{2/3-x}TiO_3$ and denied any involvement of chemical phase separation as proposed by Guiton et al.. However, their study covers a broader perspective of CB formation, using annular dark-field STEM imaging, synchrotron X-ray and neutron powder diffraction data combined with ab initio structure relaxation, particularly their detailed crystallographic analysis. Due to the presence of Li-ion, it is hard to accept this conclusion, unless a direct chemical mapping of Li-ion is provided. However, their results support Withers et al. in terms of the distribution of modulated strain due to BO_6 octahedra tilting (Figure 1.13 (c)) [55,89].

1.5.1.5 CB-like arrangements by pseudo-uniform ordering in superspace

This method to obtain CB-like microstructure is based on the pseudo-uniform distribution of minority motifs in superspace construction [61,90]. The framework of pseudo-uniform ordering can define and envisage the arrangement of minority motifs, e.g., substitutional, vacancies, interstitials, etc. Even though these strategies are based on heuristic and intuitive mathematical calculations without considering any atomic details, i.e., electronegativity, size, spin, and orbital intricacy, they have been found capable of predicting microstructural

distribution close to experimental results [61]. Pseudouniform ordering combines the Farey tree model, Repulsive lattice gas model and the Greedy lattice gas model. The former provides the basic framework of uniform distribution, whereas the latter two provide optimisation strategies. It describes the homogeneity of minority motifs in real space to compactly arrange them in the superspace construction. These descriptions are applicable only for compositionally flexible materials, where minority motifs are prone to distribute uniformly instead of arranged randomly or clustered. The inherent tendency of uniform distribution helps them to form supercells by maintaining the underlying lattice of the initial structure.

(a) Farey tree method

A given composition can be constructed hierarchically by Farey's branching rules of Farey tree model. For instance, a given composition x = n/m, can be constructed by uniform sequencing from the preceding two pairs of existing adjacent fractions (n_1/m_1 and n_2/m_2) $\rightarrow (n_1 + n_2)/(m_1 + m_2)$ as shown in Figure 1.14 (a) (upper).

(b) The repulsive lattice gas/ Greedy lattice gas

In the simplistic 1D $A_{1-x}B_x$ system, all the minority motifs 'B' (red) can be considered as 1D lattice gas as shown in Figure 1.14 (b). This lattice gas of minority motifs is expected to expand uniformly, which demonstrate uniform ordering of minority motifs in a solution made of 'A' and 'B' at a given composition. Watson described the greedy-lattice-gas (GLG) model, that it embodies an effective repulsion between minority atoms at the closest range, it does not consider the repulsion contribution from next-nearest-neighbours. In the lattice gas a pairwise repulsive interactions between the motif provide uniform distribution that brings down the total potential of the compound.

(c) Checkerboard orderings from pseudouniform ordering

Pseudouniform ordering comes into picture as the concept of repulsive uniform ordering in 1D is extended to 2D arrangement, considering all the constraints imposed by the underlying lattice. It can be understood by an example of a 2D square lattice of composition $A_{1-x}B_x$ (Figure 1.14 (d,e)).

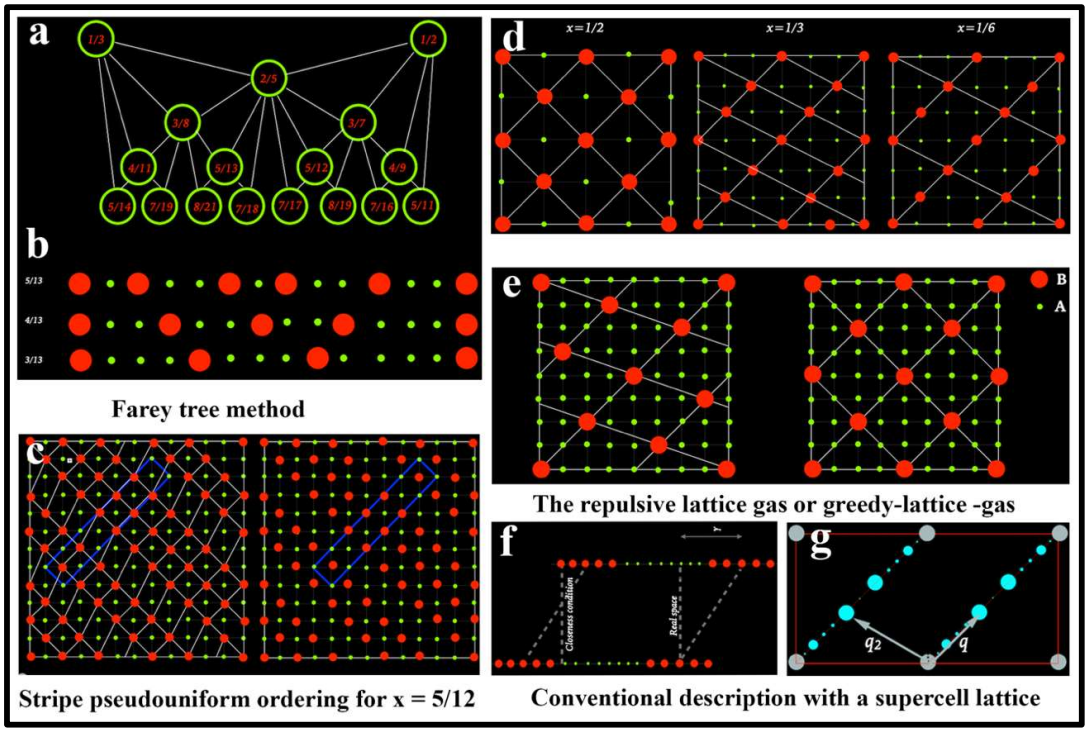

Figure 1.14: *(a) Expansion of fraction between 1/3 and 1/2 up to fifth level by Farey tree method (b) Schematic representation of Farey tree model showing 1D arrangement of minority motifs considering GLG repulsive model (c) Stripe pseudouniform ordering for x = 5/12 made after lattice stripe decomposition in a combination of two basic tiles of x = 1/2 and 1/3 (left), corresponding Farey tree sequencing 5/12: 1/2 ⊕ 1/2 ⊕ 1/3 ⊕ 1/2 ⊕ 1/3 (left), describing a supercell (right) (d) 2D tiling of x = 1:1, 1:3, 1:6 ration of solute and minority motifs (e) Although, for uniform distribution $A_{1-x}B_x$ where x =1/8 two alternative orderings are possible considering a uniform square lattice. However lattice gas model prefers former one. (f) conventional description of superspace of 1D ordering showing concatenation of monatomic columns. (g) Fourier spectra of pseudouniform stripe corresponding to x = 5/12 [61].*

The first step of pseudo uniform ordering is to apply the lattice gas repulsive model in 1D, generate the most uniform arrangements, and then develop an appropriate pair of irreducible tiles for a given stoichiometry through which the supercell is constructed. In the second step, arrange these tiles following a uniform sequencing prescribed by Farey tree rules. These tiles of two end basic concentration share a common side, and are concatenated

along the common sides, producing a pseudouniform arrangement of stripes (Figure 1.14 (c)).

These pseudouniformly distributed stripes form hierarchical intergrowth structures that follow Farey tree rule similar to 1D orderings of two different motifs. For irrational values of the composition this scheme produce incommensurately ordered stripes that are directly predictable with Farey tree model. These stripe-like arrangement converts into checkerboard ordering after providing extra dilution of minority atoms. That happens after finding an appropriate matchings among different tiles of two elementary concentration among which the actual composition is falling (Figure 1.14 (c)). Juxtapose these tiles appropriately in 2D by using a repulsive potential of some kind (repulsive Yukawa potential). This two-step organisation can generate pseudo uniform ordering, which can be seen as supercells consisting of A and B motifs. In the third step, the system achieves a final arrangement after concatenating these individual irreducible monatomic supercells (tiles) (Figure 1.15 (a)); the size of the basic monatomic supercell corresponds to the appearance of the unit fraction 1/n in the Farey composition fraction analysis [61].

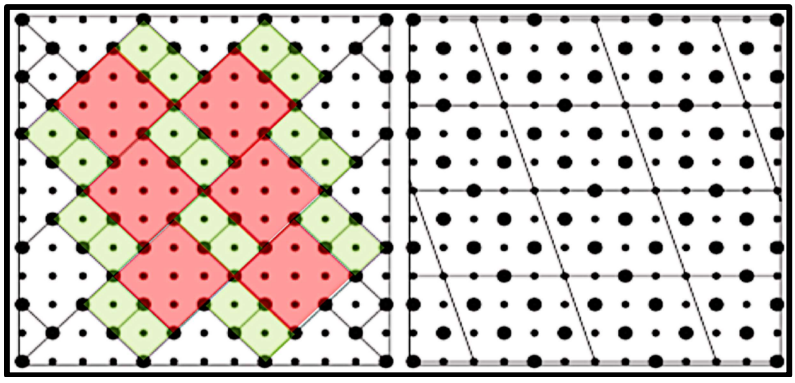

Figure 1.15: *Checkerboard-like pseudouniform orderings for x = 5/12 (a) obtained after energy optimization for larger range of the repulsive potential (b) their representation as pseudouniform arrangements of A motifs x=1/2 within a halved lattice (bcc) with a relative density of y = (1 − 2x) [61].*

In a large class of pseudouniform ordering, a quasi-one-dimensional character can be seen as interconnected stripes of two different elementary supercells, which ultimately turn into checkerboard arrangements maintaining the underlying uniformity (Figure 1.15). Even though the stripe configuration always follows the GLG criterion and tries to maximise

separation between like motifs. The checkerboard formations result from an effective repulsive interaction, intergrowth or the concatenation of basic supercells.

1.6 Applications of CB-like microstructure

Chessboard-like microstructures not only have the potential to be utilised for designing advanced electronic devices but also can bring advancement to the existing technology. A number of modern devices require directional functionality of the physical properties, e.g., memory storage devices, energy storage devices, thermoelectric devices, sensors, and detectors, whose performance can be upgraded by the evolution of CB-like microstructure. In the following section, significance of CB microstructures is given with a few examples [91].

1.6.1 High density memory applications

We are living in the computer era, where an exponentially growing demand for data storage, both in quantity and quality, inspires the development of advanced high-density memory devices. Amongst all memory storage devices, magnetic recording media is the most reliable and successful technology. A magnetic recording media requires ferromagnetic material that can retain stored magnetic signals even after removing the external magnetic field. The ability of a material to retain magnetization is called remanence. Since a recording media is expected to retain data for extended period, it should have higher coercivity (Hc). In order to increase the data storage density (Bit/inch^2), it is required to minimize the size of the smallest data storing unit (Bit). In current technology, due to the limitation of resolution and sensitivity of the reading/writing head, one bit has to cover a number of such uniformly magnetized grains covered in a rectangular area (Bit aspect ratio) (Figure 1.16). Three main technological constraints restrict the improvement of the storage density of any recording media used in PMR. First, reducing the grain size to a minimum possible limit is essential to increase storage density. Once the size of a ferromagnetic domain reduces below a critical limit, it turns into superparamagnetic, where magnetization may reverse without the application of any external applied field [92].

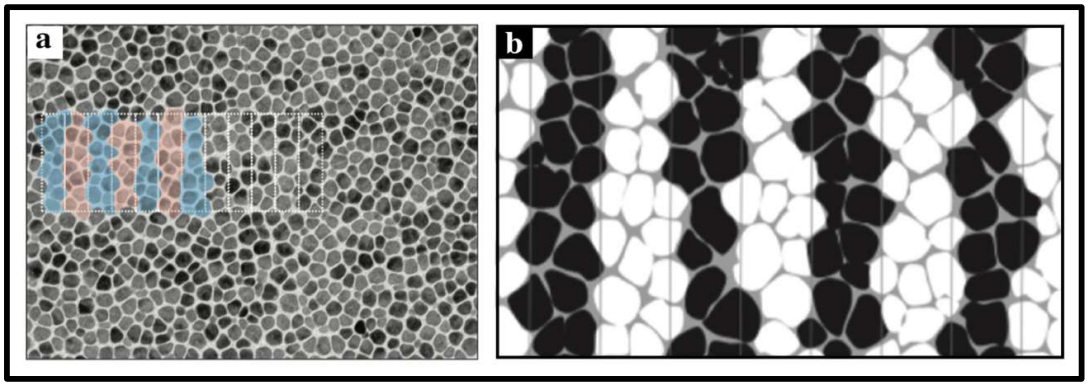

Figure 1.16: *(a) Cross-sectional SEM image of a state-of-the-art PMR media with a data storage density ~800 Gb/inch², here 1 bit is marked by white dotted lines (b) A schematic layover on an actual SEM image of a realistic media grains representing recorded transitions, where black corresponds to M = 1, white corresponds to M = −1, and grey is M = 0 [91].*

Reversal of the magnetization makes a material disqualified for storing any magnetic signal over it. Hence, there is a requirement for a constant magnetization vector for a long time; for that purpose, a superparamagnetic particle gets rejected. The reversal of the magnetization can be decreased by introducing high magnetic anisotropy in the recording media. Second, achieving higher magnetic anisotropy without compromising the writing capacity of the recording head. The magnetic anisotropy energy of the recording media cannot be higher than a limit because the saturation magnetization limits the field exerted by the writing head. Higher magnetic anisotropy allows for a decrease in grain size beyond a limit without turning superparamagnetic. Magnetic anisotropy can be obtained in many ways, e.g., shape anisotropy, reduced exchange coupling between the magnetic grains, magnetic soft underlayers, adjusting magnetic response of surrounding grains (exchange decupling) [91]. Therefore, better methods are needed to separate the magnetic grains from each other. Third, the non-uniform irregular shape of the magnetic grains (Figure 1.16(a)) creates jittering (loss of data on reading and writing) because sometimes the electronic head cannot cover the whole area of grains that are situated at the edge. Hence, it is crucial to have faceted grains of uniform size to enhance the efficiency of the storage material.

These mutually dependent limitations of a recording media are called a recording trilemma. This trilemma can be solved only by adopting some design ingenuity [91]. However, there is a lot of advancements made so far in order to overcome the above-mentioned limitations of a material to be utilized in high-density memory storage device. In this context

development of magnetic chessboard-like microstructure is an alternative arrangement of two cuboidal magnetic domains with different magnetic sensitivity, i.e., ferromagnetic and paramagnetic (Figure 1.11) [1,93]. It is reported that compositional segregation can obtain exchange decoupling at high temperatures [94]. A material consisting of a well-organized mixture of two phases possessing different magnetic properties can obtain a better decoupling effect by reducing the exchange coupling. In addition, magnetic anisotropy can be introduced in the microstructure by introducing the crystal or shape anisotropy due to the formation of rods like magnetic domains in both the Fe-rich and Mn-rich domains. Hence, all the above-mentioned discrepancies can be removed by utilizing a recording media with a chessboard-like microstructure, developed in Mn-doped $CoFe_2O_4$ and $CoFeGaZnO_4$. CB-like microstructure developed in the above-mentioned spinels evolve with a 3D alternative distribution of cuboidal nanodomains with different magnetic properties, i.e., ferromagnetic (Fe-rich domain), paramagnetic (Mn-rich domain) or antiferromagnetic (in case of mixed chemistry domains). It is well documented that in the Mn-doped $CoFe_2O_4$ system, the coercivity increases four times after a magnetic CB-like microstructure evolution. This CB-like microstructure can facilitate magnetisation reversal by developing a nonmagnetic domain surrounding the ferromagnetic domain [95]. On the other hand, the rectangular/square shape of the domains (Figure 1.11(d)) may help in improving data efficiency [96].

1.6.2 Thermoelectric applications

CB-like microstructures may also be utilised for thermoelectric applications. Well-organised CB-like nanodomains developed in ZnMnGaO4 oxide systems can reduce the material's thermal conductivity beyond the theoretical minimum limit of the corresponding bulk material consisting of similar phases. Such materials can be utilised for advanced thermoelectric oxides. Nanochessboard-like microstructures are expected to be applicable in thermoelectric applications with higher electrical conductivities in combination to lower thermal conductivity [4].

1.6.3 Applications of self-assembled 3-D CB microstructure in ASSLBs

All-solid-state lithium-ion batteries (ASSLBs) have emerged as a panacea for most of the technical issues that restrict conventional Li-ion batteries in fulfilling the current expectations with an energy storage device. Conventional batteries with liquid and polymer electrolytes suffer from chemical and thermal instability, physical venerability, leakage and

shorting, etc. Most of these concerns can be resolved by using non-flammable and chemically improved inorganic solid-state electrolytes [97]. However, there are still few areas where ASSLBs have a lot of scope for improvement, such as interface delamination [98], chemical phase stability [99] and charge recombination, etc.[100]. These issues become more severe for elevated temperature applications (>400) [101]. In ASSLBs, electrode delamination happens due to interfacial decomposition and expansion-contraction of both the solid-state electrolyte and electrodes during charging and discharging [102,103]. Hence, designing an inorganic conductor with efficient ionic conductivity, minimum electronic conductivity and structural stability is a prodigious task. Here some challenges are enlisted, which should be mitigated:

1. Development of proper conduction channels, interconnected vacancies and interstitial sites with low migration barrier energy to minimise charge recombination for improved percolation of ions.
2. Designing a material that can preserve structural integrity up to a large number of cyclic charging and discharging with weak interaction forces between the mobile ions and the framework.
3. Improved conductivity by increasing bottleneck diameter and minimizing the grain boundary effects.

This aim is partially achievable by utilising a material as solid state electrolyte and electrode with a well-organised phase-separated microstructure. In this microstructure, one phase provides easy path way for ion migration and the other phase provides the structural integrity. Such microstructure in a solid-state electrolyte can be achieved by applying suitable techniques such as (i) substitution of aliovalent cations [84,85] (ii) Spinodal decomposition [13,71] (iii) CB-like microstructural evolution [19,24,104,105] (iv) ionic and vacancy ordering to obtain optimum site sizes and diffusion channels for Li-ion [32].

A structure that provides an optimum ratio of Li^+ ion and vacancies with a shortest path way to channelize Li^+ ions through three-dimensionally linked vacancies is considered as suitable for solid state electrodes (SSEs). A-site deficient perovskite oxides containing Li^+ have received attention due to their significant Li^+ conductivity [100]. Among all promising oxides, perovskite-based systems have got lot of attention due to its high lithium-ion conductivity at room temperature. Among all, $Li_{3x}La_{(2/3)-x}\square_{(1/3)-2x}TiO_3$ x~0.16 (LLTO) is

best as reported by Inaguma et.al, with an ionic conductivity of the order of 10^{-3} Scm^{-1}[85]. In perovskites, "bottleneck," is located in the space between two adjacent A-sites that is surrounded by four oxygen atoms. Modification in the crystal structure by any mean leads to a varied bottleneck diameter and if somehow this diameter becomes large enough to let the Li^{+} ion flow smoothly by a shortest route, ionic conductivity improves significantly. Usually in any crystal structure the bottleneck diameter can be enlarged by increasing the lattice parameter [106]. Additionally, minimizing the charge recombination is also needed for improved electrochemical properties desired for battery application. It is possible to fabricate a microstructure consisting of well separated Li conducting phase and Li lean phase to provide separate charge carrier transportation. Such microstructures can be fabricated by bottom-up techniques and phase transformation. Spinodal decomposition is one of those techniques by which such microstructure consisting of Li-rich and Li-lean phases can be designed. Evolution of chessboard-like microstructure in lanthanide based perovskites ($LiLnTiO_3$, Ln= La, Nd, Pr etc.)[107], appears to satisfy most of the above-mentioned requirements.

The research work, reported in the thesis is derived from designing such novel multifunctional materials based on CB-like microstructures. An attempt has been made to understand the evolution mechanism of CB-like microstructure evolution in oxides.

References

[1] C.L. Zhang, S. Yeo, Y. Horibe, Y.J. Choi, S. Guha, M. Croft, S.-W. Cheong, S. Mori, Coercivity and nanostructure in magnetic spinel $Mg(Mn,Fe)_2O_4$, Appl. Phys. Lett. 90 (2007) 133123. https://doi.org/10.1063/1.2717568.

[2] H. Zheng, J. Wang, S.E. Lofland, Z. Ma, L. Mohaddes-Ardabili, T. Zhao, L. Salamanca-Riba, S.R. Shinde, S.B. Ogale, F. Bai, D. Viehland, Y. Jia, D.G. Schlom, M. Wuttig, A. Roytburd, R. Ramesh, Multiferroic $BaTiO_3$-$CoFe_2O_4$ nanostructures, Science (5658) 303 (2004) 661–663. https://doi.org/10.1126/science.1094207.

[3] D. Seetharamdoo, Resonant negative refractive index metamaterials, in: metamaterial, InTech, 2012: pp. 28–35. https://doi.org/10.5772/35153.

[4] A. Kosuga, K. Kurosaki, K. Yubuta, A. Charoenphakdee, S. Yamanaka, R. Funahashi, Solid-state self-assembly of nanostructured oxide as a candidate high-performance thermoelectric material, J. Electron. Mater. 38 (2009) 1303–1308. https://doi.org/10.1007/s11664-009-0716-4.

[5] S. Park, Y. Horibe, T. Asada, L.S. Wielunski, N. Lee, P.L. Bonanno, S.M. O'Malley, A.A. Sirenko, A. Kazimirov, M. Tanimura, T. Gustafsson, S.-W. Cheong, Highly aligned epitaxial nanorods with a checkerboard pattern in oxide films, Nano Lett. 8 (2008) 720–724. https://doi.org/10.1021/nl072848s.

[6] N.I. Zheludev, Y.S. Kivshar, From metamaterials to metadevices, Nat. Mater. 11 (2012) 917–924. https://doi.org/10.1038/nmat3431.

[7] Y. Liu, X. Zhang, Metamaterials: a new frontier of science and technology, Chem. Soc. Rev. 40 (2011) 2494. https://doi.org/10.1039/c0cs00184h.

[8] C.L. Zhang, C.M. Tseng, C.H. Chen, S. Yeo, Y.J. Choi, S.-W. Cheong, Magnetic nanocheckerboards with tunable sizes in the Mn-doped $CoFe_2O_4$ spinel, Appl. Phys. Lett. 91 (2007) 233110. https://doi.org/10.1063/1.2821838.

[9] K. Ariga, M. Nishikawa, T. Mori, J. Takeya, L.K. Shrestha, J.P. Hill, Self-assembly as a key player for materials nanoarchitectonics, Sci. Technol. Adv. Mater. 20 (2019) 51–95. https://doi.org/10.1080/14686996.2018.1553108.

[10] M. Wild, S. Berner, H. Suzuki, L. Ramoino, A. Baratoff, T.A. Junga, Molecular assembly and self-assembly: molecular nanoscience for future technologies, Ann. N. Y. Acad. Sci. 1006 (2003) 291–305. https://doi.org/10.1196/annals.1292.020.

[11] E.V. Amadi, A. Venkataraman, C. Papadopoulos, Nanoscale self-assembly: concepts, applications and challenges, Nanotechnology. 33 (2022) 132001.

https://doi.org/10.1088/1361-6528/ac3f54.

[12] K.K. Bharathi, H. Tan, S. Takeuchi, L. Meshi, H. Shen, J. Shin, I. Takeuchi, L.A. Bendersky, Effect of oxygen pressure on structure and ionic conductivity of epitaxial $Li_{0.33}La_{0.55}TiO_3$ solid electrolyte thin films produced by pulsed laser deposition, RSC Adv. 6 (2016) 61974–61983. https://doi.org/10.1039/C6RA12879C.

[13] E.P. Butler, G. Thomas, Structure and properties of spinodally decomposed Cu-Ni-Fe alloys, Acta Metall. 18 (1970) 347–365. https://doi.org/10.1016/0001-6160(70)90150-1.

[14] K.I. Udoh, A.M. El Araby, Y. Tanaka, K. Hisatsune, K. Yasuda, G. Van Tendeloo, J. Van Landuyt, Structural aspects of AuCu I or AuCu II and a cuboidal block configuration of f.c.c. disordered phase in AuCu-Pt and AuCu-Ag pseudobinary alloys, Mater. Sci. Eng. A. 203 (1995) 154–164. https://doi.org/10.1016/0921-5093(95)09850-X.

[15] Y. Le Bouar, A. Loiseau, A.G. Khachaturyan, Origin of chessboard-like structures in decomposing alloys. Theoretical model and computer simulation, Acta Mater. 46 (1998) 2777–2788. https://doi.org/10.1016/S1359-6454(97)00455-2.

[16] A. Artemev, Y. Jin, A.G. Khachaturyan, Three-dimensional phase field model of proper martensitic transformation, Acta Mater. 49 (2001) 1165–1177. https://doi.org/10.1016/S1359-6454(01)00021-0.

[17] P.K. Davies, M. Akaogi, Phase intergrowths in spinelloids, Nature. 305 (1983) 788–790. https://doi.org/10.1038/305788a0.

[18] S. Yeo, Y. Horibe, S. Mori, C.M. Tseng, C.H. Chen, A.G. Khachaturyan, C.L. Zhang, S.-W. Cheong, Solid state self-assembly of nanocheckerboards, Appl. Phys. Lett. 89 (2006) 233120. https://doi.org/10.1063/1.2402115.

[19] B.S. Guiton, P.K. Davies, Nano-chessboard superlattices formed by spontaneous phase separation in oxides, Nat. Mater. 6 (2007) 586–591. https://doi.org/10.1038/nmat1953.

[20] S. Skink, Encyclopedia of nanotechnology, Springer Netherlands, Dordrecht, 2012. https://doi.org/10.1007/978-90-481-9751-4.

[21] Y. Ni, W. Rao, A.G. Khachaturyan, Pseudospinodal mode of decomposition in films and formation of chessboard-like nanostructure, Nano Lett. 9 (2009) 3275–3281. https://doi.org/10.1021/nl901551j.

[22] H. Zeng, P.M. Rice, S.X. Wang, S. Sun, Shape-controlled synthesis and shape-induced texture of $MnFe_2O_4$ nanoparticles, J. Am. Chem. Soc. 126 (2004) 11458–

11459. https://doi.org/10.1021/ja045911d.

[23] S. Yeo, S. Guha, S.W. Cheong, Generic properties of Mn spinels with an immiscibility induced by a Jahn–Teller distortion, J. Phys. Condens. Matter. 21 (2009) 125402. https://doi.org/10.1088/0953-8984/21/12/125402.

[24] P.M. Woodward, A chessboard at the nanoscale, Nat. Mater. 6 (2007) 549–551. https://doi.org/10.1038/nmat1970.

[25] Y. Ni, A.G. Khachaturyan, From chessboard tweed to chessboard nanowire structure during pseudospinodal decomposition, Nat. Mater. 8 (2009) 410–414. https://doi.org/10.1038/nmat2431.

[26] W. Hresko, Feature Article, Remedial Spec. Educ. 10 (1989) 8–8. https://doi.org/10.1177/074193258901000304.

[27] E. Cara, F. Ferrarese Lupi, M. Fretto, N. De Leo, M. Tortello, R. Gonnelli, K. Sparnacci, L. Boarino, Directed self-assembly of polystyrene nanospheres by direct Laser-writing lithography, Nanomaterials. 10 (2020) 280. https://doi.org/10.3390/nano10020280.

[28] F. Yang, X. Wang, D. Zhang, J. Yang, D. Luo, Z. Xu, J. Wei, J.-Q. Wang, Z. Xu, F. Peng, X. Li, R. Li, Y. Li, M. Li, X. Bai, F. Ding, Y. Li, Chirality-specific growth of single-walled carbon nanotubes on solid alloy catalysts, Nature. 510 (2014) 522–524. https://doi.org/10.1038/nature13434.

[29] P.W.K. Rothemund, Folding DNA to create nanoscale shapes and patterns, Nature. 440 (2006) 297–302. https://doi.org/10.1038/nature04586.

[30] D.B. Dement, M.K. Quan, V.E. Ferry, Nanoscale patterning of colloidal nanocrystal films for nanophotonic applications using direct write electron beam lithography, ACS Appl. Mater. Interfaces. 11 (2019) 14970–14979. https://doi.org/10.1021/acsami.9b01159.

[31] Y. Suzuki, M. Endo, H. Sugiyama, Lipid-bilayer-assisted two-dimensional self-assembly of DNA origami nanostructures, Nat. Commun. 6 (2015) 8052. https://doi.org/10.1038/ncomms9052.

[32] S. García-Martín, M.A. Alario-Franco, H. Ehrenberg, J. Rodríguez-Carvajal, U. Amador, Crystal structure and microstructure of some $La_{2/3-x}Li_{3x}TiO_3$ oxides: An example of the complementary use of electron diffraction and microscopy and synchrotron X-ray diffraction to study complex materials, J. Am. Chem. Soc. 126 (2004) 3587–3596. https://doi.org/10.1021/ja038410l.

[33] B.S. Guiton, H. Wu, P.K. Davies, Neutron powder diffraction of $(Nd_{7/12}Li_{1/4})TiO_3$

nano-checkerboard superlattices, Chem. Mater. 20 (2008) 2860–2862. https://doi.org/10.1021/cm800473m.

[34] A. Demortière, A. Snezhko, M. V. Sapozhnikov, N. Becker, T. Proslier, I.S. Aranson, Self-assembled tunable networks of sticky colloidal particles, Nat. Commun. 5 (2014) 3117. https://doi.org/10.1038/ncomms4117.

[35] M. Ohno, S. Mori, Y. Togawa, Y. Horibe, Magnetic chessboard-type nanodomains in Mn-doped CoFe 2 O 4, IOP Conf. Ser. Mater. Sci. Eng. 18 (2011) 092052. https://doi.org/10.1088/1757-899X/18/9/092052.

[36] B.A. Grzybowski, C.E. Wilmer, J. Kim, K.P. Browne, K.J.M. Bishop, Self-assembly: from crystals to cells, Soft Matter. 5 (2009) 1110. https://doi.org/10.1039/b819321p.

[37] K. Ariga, J.P. Hill, M. V. Lee, A. Vinu, R. Charvet, S. Acharya, Challenges and breakthroughs in recent research on self-assembly, Sci. Technol. Adv. Mater. 9 (2008) 014109. https://doi.org/10.1088/1468-6996/9/1/014109.

[38] R.J. Celotta, S.B. Balakirsky, A.P. Fein, F.M. Hess, G.M. Rutter, J.A. Stroscio, Invited Article: Autonomous assembly of atomically perfect nanostructures using a scanning tunneling microscope, Rev. Sci. Instrum. 85 (2014) 121301. https://doi.org/10.1063/1.4902536.

[39] J.M. Smith, H.C. Van Ness, M.M. Abbot, M.T.. Swihart, Introduction to chemical engineering thermodynamics eight edition, 2018.

[40] K.J.M. Bishop, C.E. Wilmer, S. Soh, B.A. Grzybowski, Nanoscale forces and their uses in self-assembly, Small. 5 (2009) 1600–1630. https://doi.org/10.1002/smll.200900358.

[41] G. Singh, R. Ni, A. Marwaha, A review of metamaterials and its applications, Int. J. Eng. Trends Technol. 19 (2015) 305–310. https://doi.org/10.14445/22315381/IJETT-V19P254.

[42] P. Rodgers, Chip maker turns to self-assembly, Nat. Nanotechnol. (2007). https://doi.org/10.1038/nnano.2007.170.

[43] G. Markovich, C.P. Collier, S.E. Henrichs, F. Remacle, R.D. Levine, J.R. Heath, Architectonic quantum dot solids, Acc. Chem. Res. 32 (1999) 415–423. https://doi.org/10.1021/ar980039x.

[44] Y. Fang, A. Prominski, M.Y. Rotenberg, L. Meng, H. Acarón Ledesma, Y. Lv, J. Yue, E. Schaumann, J. Jeong, N. Yamamoto, Y. Jiang, B. Elbaz, W. Wei, B. Tian, Micelle-enabled self-assembly of porous and monolithic carbon membranes for

bioelectronic interfaces, Nat. Nanotechnol. 16 (2021) 206–213. https://doi.org/10.1038/s41565-020-00805-z.

[45] R. Yi, Y. Mao, Y. Shen, L. Chen, Self-Assembled Monolayers for Batteries, J. Am. Chem. Soc. 143 (2021) 12897–12912. https://doi.org/10.1021/jacs.1c04416.

[46] J.G. Werner, G.G. Rodríguez-Calero, H.D. Abruña, U. Wiesner, Block copolymer derived 3-D interpenetrating multifunctional gyroidal nanohybrids for electrical energy storage, Energy Environ. Sci. 11 (2018) 1261–1270. https://doi.org/10.1039/C7EE03571C.

[47] J.C. Bose, On the rotation of plane of polarisation of electric wave by a twisted structure, Proc. R. Soc. London. 63 (1898) 146–152. https://doi.org/10.1098/rspl.1898.0019.

[48] V.G. Veselago, The electrodynamics of substances with simultaneously negative values of ε and μ, Sov. Phys. Uspekhi. 10 (1968) 509–514. https://doi.org/10.1070/PU1968v010n04ABEH003699.

[49] Z. Chen, B. Guo, Y. Yang, C. Cheng, Metamaterials-based enhanced energy harvesting: A review, Phys. B Condens. Matter. 438 (2014) 1–8. https://doi.org/10.1016/j.physb.2013.12.040.

[50] S. Dey, C. Fan, K. V. Gothelf, J. Li, C. Lin, L. Liu, N. Liu, M.A.D. Nijenhuis, B. Saccà, F.C. Simmel, H. Yan, P. Zhan, DNA origami, Nat. Rev. Methods Prim. 1 (2021) 13. https://doi.org/10.1038/s43586-020-00009-8.

[51] Z.W. Wang, Z. Wang, Y.J. Song, C. Ma, Y. Cai, Z. Chen, H.F. Tian, H.X. Yang, G.-F. Chen, J.Q. Li, Structural phase separation in $K_{0.8}Fe_{1.6+x}Se_2$ Superconductors, J. Phys. Chem. C. 116 (2012) 17847–17852. https://doi.org/10.1021/jp306310m.

[52] S. García-Martin, F. García-Alvarado, A.D. Robertson, A.R. West, M.A. Alario-Franco, Microstructural Study of the Li+Ion Substituted Perovskites $Li_{0.5-3x}Nd_{0.5+x}TiO_3$, J. Solid State Chem. 128 (1997) 97–101. https://doi.org/10.1006/jssc.1996.7173.

[53] C. Leroux, A. Loiseau, D. Broddin, G. Vantendeloo, Electron microscopy study of the coherent two-phase mixtures $L1_0$ + $L1_2$, in Co–Pt alloys, Philos. Mag. B. 64 (1991) 57–82. https://doi.org/10.1080/13642819108207603.

[54] E.P. Favvas, A.C. Mitropoulos, What is spinodal decomposition?, J. Eng. Sci. Technol. Rev. 1 (2008) 25–27. https://doi.org/10.25103/jestr.011.05.

[55] A.M. Abakumov, R. Erni, A.A. Tsirlin, M.D. Rossell, D. Batuk, G. Nénert, G. Van Tendeloo, Frustrated octahedral tilting distortion in the incommensurately

modulated $Li_{3x}Nd_{2/3-x}TiO_3$ perovskites, Chem. Mater. 25 (2013) 2670–2683. https://doi.org/10.1021/cm4012052.

[56] M.S. Senn, J.P. Wright, J.P. Attfield, Charge order and three-site distortions in the Verwey structure of magnetite, Nature. 481 (2012) 173–176. https://doi.org/10.1038/nature10704.

[57] G. Tendeloo, D. Schryvers, L.E. Tanner, D. Broddin, C. Ricolleau, A. Loiseau, Structural phase transformations in alloys: an electron microscopy study, in: Struct. Phase Stab. Alloy., Springer US, Boston, MA, 1992: pp. 219–229. https://doi.org/10.1007/978-1-4615-3382-5_14.

[58] P. Giraldo-Gallo, Y. Zhang, C. Parra, H.C. Manoharan, M.R. Beasley, T.H. Geballe, M.J. Kramer, I.R. Fisher, Stripe-like nanoscale structural phase separation in superconducting $BaPb_{1-x}Bi_xO_3$, Nat. Commun. 6 (2015) 8231. https://doi.org/10.1038/ncomms9231.

[59] M. Uehara, S.-W. Cheong, Relaxation between charge order and ferromagnetism in manganites: Indication of structural phase separation, Europhys. Lett. 52 (2000) 674–680. https://doi.org/10.1209/epl/i2000-00491-5.

[60] W. Hume-Rothery, H.M. Powell, On the Theory of super-lattice structures in alloys, Zeitschrift Für Krist. - Cryst. Mater. 91 (1935) 23–47. https://doi.org/10.1524/zkri.1935.91.1.23.

[61] S. González, J.M. Perez-Mato, L. Elcoro, A. García, Superlattice pseudouniform orderings as modulated structures: Stripe and checkerboard arrangements, Phys. Rev. B. 84 (2011) 184106. https://doi.org/10.1103/PhysRevB.84.184106.

[62] N. Wagner, R. Seshadri, J.M. Rondinelli, Property control from polyhedral connectivity in ABO_3 oxides, Phys. Rev. B. 100 (2019) 064101. https://doi.org/10.1103/PhysRevB.100.064101.

[63] H. Bethe, Termaufspaltung in kristallen, Ann. Phys. 395 (1929) 133–208. https://doi.org/10.1002/andp.19293950202.

[64] J.H. Van Vleck, Theory of the variations in paramagnetic anisotropy among different salts of the iron group, Phys. Rev. 41 (1932) 208–215. https://doi.org/10.1103/PhysRev.41.208.

[65] A.J. Bradley, H. Lipson, An X-ray investigation of slowly cooled copper-nickel-aluminium alloys, Proc. R. Soc. London. Ser. A. Math. Phys. Sci. 167 (1938) 421–438. https://doi.org/10.1098/rspa.1938.0139.

[66] V. Daniel, H. Lipson, An X-ray study of the dissociation of an alloy of copper, iron

and nickel, Proc. R. Soc. London. Ser. A. Math. Phys. Sci. 181 (1943) 368–378. https://doi.org/10.1098/rspa.1943.0014.

[67] D.A. Porter, K.E. Easterling, K.E. Easterling, Phase transformations in metals and alloys (revised reprint), CRC Press, 2009. https://doi.org/10.1201/9781439883570.

[68] K.U.V. Jirapure S.C., Borade A.B., A new approach of strengthening-spinodal decomposition, Int. J. Appl. Sci. Eng. Res. 4 (2015) 77–85. https://doi.org/10.6088/ijaser.04008.

[69] M.R. Hoare, P. Pal, Physical cluster mechanics: Statistical thermodynamics and nucleation theory for monatomic systems, Adv. Phys. 24 (1975) 645–678. https://doi.org/10.1080/00018737500101481.

[70] J.W. Cahn, On spinodal decomposition in cubic crystals, Acta Metall. 10 (1962) 179–183. https://doi.org/10.1016/0001-6160(62)90114-1.

[71] J.W. Cahn, On spinodal decomposition, Acta Metall. 9 (1961) 795–801. https://doi.org/10.1016/0001-6160(61)90182-1.

[72] G. Tammann, Zum Gedächtnis der Entdeckung des Isomorphismus vor 100 Jahren. Die chemischen und galvanischen Eigenschaften von Mischkristallreihen und ihre Atomverteilung, Zeitschrift Für Anorg. Und Allg. Chemie. 107 (1919) 1–239. https://doi.org/10.1002/zaac.19191070102.

[73] H. Matsuda, K. Oki, S. Kiyoto, T. Eguchi, Order-disorder transformations in Fe-Al alloys, J. Japan Inst. Met. 31 (1967) 1321–1326. https://doi.org/10.2320/jinstmet1952.31.12_1321.

[74] R. Kikuchi, J.W. Cahn, Theory of interphase and antiphase boundaries in f.c.c. alloys, Acta Metall. 27 (1979) 1337–1353. https://doi.org/10.1016/0001-6160(79)90203-7.

[75] K.C. Thompson-Russell, J.W. Edington, Electron Microscope Specimen Preparation Techniques in Materials Science, Macmillan Education UK, London, 1977. https://doi.org/10.1007/978-1-349-03403-1.

[76] E.J.W. Verwey, P.W. Haayman, Electronic conductivity and transition point of magnetite ("Fe_3O_4"), Physica. 8 (1941) 979–987. https://doi.org/10.1016/S0031-8914(41)80005-6.

[77] Y. Inaguma, C. Liquan, M. Itoh, T. Nakamura, T. Uchida, H. Ikuta, M. Wakihara, High ionic conductivity in lithium lanthanum titanate, Solid State Commun. 86 (1993) 689–693. https://doi.org/10.1016/0038-1098(93)90841-A.

[78] J.B. Goodenough, Electronic structure of CMR manganites (invited), J. Appl. Phys.

81 (1997) 5330–5335. https://doi.org/10.1063/1.364536.

[79] M. Uehara, S. Mori, C.H. Chen, S.W. Cheong, Percolative phase separation underlies colossal magnetoresistance in mixed-valent manganites, Nature. 399 (1999) 560–563. https://doi.org/10.1038/21142.

[80] J. Khatua, T. Arh, S.B. Mishra, H. Luetkens, A. Zorko, B. Sana, M.S.R. Rao, B.R.K. Nanda, P. Khuntia, Development of short and long-range magnetic order in the double perovskite based frustrated triangular lattice antiferromagnet Ba_2MnTeO_6, Sci. Rep. 11 (2021) 6959. https://doi.org/10.1038/s41598-021-84876-5.

[81] K.H. Hong, A.M. Arevalo-Lopez, J. Cumby, C. Ritter, J.P. Attfield, Long range electronic phase separation in $CaFe_3O_5$, Nat. Commun. 9 (2018) 2975. https://doi.org/10.1038/s41467-018-05363-6.

[82] A. Yakubovskii, A. Trokiner, S. Verkhovskii, A. Gerashenko, D. Khomskii, Charge and orbital ordering in $Pr_{0.5}Ca_{0.5}MnO_3$ studied by 17O NMR, Phys. Rev. B. 67 (2003) 064414. https://doi.org/10.1103/PhysRevB.67.064414.

[83] M. Guymont, R. Portier, D. Gratiads, Guymonmt, Porti, Inst. Phys. Conf. Ser. 61 (1982) 387.

[84] Y. Inaguma, J. Yu, Y. Shan, M. Itoh, T. Nakamuraa, The effect of the hydrostatic pressure on the ionic conductivity in a perovskite lanthanum lithium titanate, J. Electrochem. Soc. 142 (1995) L8–L11. https://doi.org/10.1149/1.2043988.

[85] Y. Inaguma, C. Liquan, M. Itoh, T. Nakamura, T. Uchida, H. Ikuta, M. Wakihara, High ionic conductivity in lithium lanthanum titanate, Solid State Commun. 86 (1993) 689–693. https://doi.org/10.1016/0038-1098(93)90841-A.

[86] J.-L. Ortiz-Quiñonez, L. García-González, F.E. Cancino-Gordillo, U. Pal, Particle dispersion and lattice distortion induced magnetic behavior of $La_{1-x}Sr_xMnO_3$ perovskite nanoparticles grown by salt-assisted solid-state synthesis, Mater. Chem. Phys. 246 (2020) 122834. https://doi.org/10.1016/j.matchemphys.2020.122834.

[87] M. Itoh, Y. Inaguma, W. Jung, L. Chen, T. Nakamura, High lithium ion conductivity in the perovskite-type compounds, Solid State Ionics. 70–71 (1994) 203–207. https://doi.org/10.1016/0167-2738(94)90310-7.

[88] B.S. Guiton, P.K. Davies, Spontaneous compositional nanopatterning in Li-containing perovskite oxides, J. Am. Chem. Soc. 130 (2008) 17168–17173. https://doi.org/10.1021/ja806130u.

[89] R.L. Withers, L. Bourgeois, A. Snashall, Y. Liu, L. Norén, C. Dwyer, J. Etheridge, Chessboard/Diamond nanostructures and the A-site deficient, $Li_{1/2-3x}Nd_{1/2+x}TiO_3$,

defect perovskite solid solution, Chem. Mater. 25 (2013) 190–201. https://doi.org/10.1021/cm303239d.

[90] S. González, J.M. Perez-Mato, L. Elcoro, A. García, R.L. Withers, L. Bourgeois, Compositional uniformity, domain patterning and the mechanism underlying nano-chessboard arrays, J. Phys. Condens. Matter. 24 (2012) 495301. https://doi.org/10.1088/0953-8984/24/49/495301.

[91] F.C. Gaspare Varvaro, Ultra-High-Density magnetic recording, Jenny Stanford Publishing, 2016. https://doi.org/10.1201/b20044.

[92] R. Skomski, Simple models of magnetism, Oxford University Press, 2008. https://doi.org/10.1093/acprof:oso/9780198570752.001.0001.

[93] Y. Horibe, S. Takeyama, S. Mori, Large-scale phase separation with nano-twin domains in manganite spinel $(Co,Fe,Mn)_3O_4$, in: AIP Conf. Proc., 2016: p. 050005. https://doi.org/10.1063/1.4961358.

[94] J.H. Lee, L. Fang, E. Vlahos, X. Ke, Y.W. Jung, L.F. Kourkoutis, J.W. Kim, P.J. Ryan, T. Heeg, M. Roeckerath, V. Goian, M. Bernhagen, R. Uecker, P.C. Hammel, K.M. Rabe, S. Kamba, J. Schubert, J.W. Freeland, D.A. Muller, C.J. Fennie, P. Schiffer, V. Gopalan, E. Johnston-Halperin, D.G. Schlom, A strong ferroelectric ferromagnet created by means of spin–lattice coupling, Nature. 466 (2010) 954–958. https://doi.org/10.1038/nature09331.

[95] Anisotropy and Magnetostriction in magnetic oxides: Journal of Applied Physics: Vol 32, No 3, (n.d.).

[96] S.N. Piramanayagam, Perpendicular recording media for hard disk drives, J. Appl. Phys. 102 (2007) 011301. https://doi.org/10.1063/1.2750414.

[97] R. Schmuch, R. Wagner, G. Hörpel, T. Placke, M. Winter, Performance and cost of materials for lithium-based rechargeable automotive batteries, Nat. Energy. 3 (2018) 267–278. https://doi.org/10.1038/s41560-018-0107-2.

[98] J.F.M. Oudenhoven, L. Baggetto, P.H.L. Notten, All-solid-state lithium-ion microbatteries: a review of various three-dimensional concepts, Adv. Energy Mater. 1 (2011) 10–33. https://doi.org/10.1002/aenm.201000002.

[99] S. Chandrashekar, N.M. Trease, H.J. Chang, L.-S. Du, C.P. Grey, A. Jerschow, Li MRI of Li batteries reveals location of microstructural lithium, Nat. Mater. 11 (2012) 311–315. https://doi.org/10.1038/nmat3246.

[100] Z. Zhang, Y. Shao, B. Lotsch, Y.S. Hu, H. Li, J. Janek, L.F. Nazar, C.W. Nan, J. Maier, M. Armand, L. Chen, New horizons for inorganic solid state ion conductors,

Energy Environ. Sci. 11 (2018) 1945–1976. https://doi.org/10.1039/C8EE01053F.

[101] B. Dunn, H. Kamath, J.M. Tarascon, Electrical energy storage for the grid: a battery of choices, Science (6058) 334 (2011) 928–935. https://doi.org/10.1126/science.1212741.

[102] W. Zhang, D.A. Weber, H. Weigand, T. Arlt, I. Manke, D. Schröder, R. Koerver, T. Leichtweiss, P. Hartmann, W.G. Zeier, J. Janek, Interfacial processes and influence of composite cathode microstructure controlling the performance of all-solid-state lithium batteries, ACS Appl. Mater. Interfaces. 9 (2017) 17835–17845. https://doi.org/10.1021/acsami.7b01137.

[103] R. Koerver, I. Aygün, T. Leichtweiß, C. Dietrich, W. Zhang, J.O. Binder, P. Hartmann, W.G. Zeier, J. Janek, Capacity Fade in Solid-State Batteries: Interphase formation and chemomechanical processes in nickel-rich layered oxide cathodes and lithium thiophosphate solid electrolytes, Chem. Mater. 29 (2017) 5574–5582. https://doi.org/10.1021/acs.chemmater.7b00931.

[104] G. King, S. Garcia-Martin, P.M. Woodward, Octahedral tilt twinning and compositional modulation in $NaLaMgWO_6$, Acta Crystallogr. Sect. B Struct. Sci. 65 (2009) 676–683. https://doi.org/10.1107/S0108768109032728.

[105] N. Research, 2008, 20, 2860–2862, Communications. (2008) 2860–2862.

[106] S. Stramare, V. Thangadurai, W. Weppner, Lithium lanthanum titanates: a review, Chem. Mater. 15 (2003) 3974–3990. https://doi.org/10.1021/cm0300516.

[107] R. Erni, A.M. Abakumov, M.D. Rossell, D. Batuk, A.A. Tsirlin, G. Nénert, G. Van Tendeloo, Nanoscale phase separation in perovskites revisited, Nat. Mater. 13 (2014) 216–217. https://doi.org/10.1038/nmat3865.